Spectroscopy and Magnetism

Michaelmas Term 2024

Contents

1 Electronic Spectroscopy of Metal Complexes

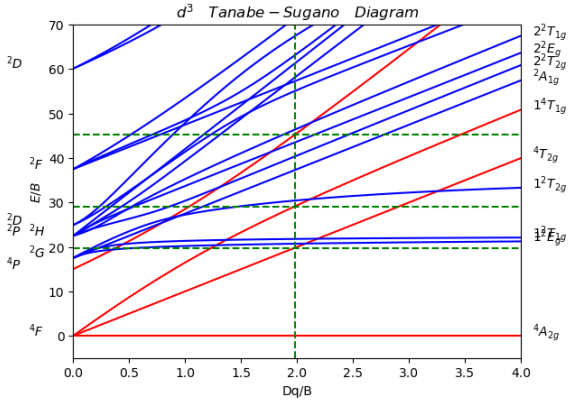

Bibliography:
All general inorganic texts give a basic coverage of electronic spectroscopy. For more specialised reading, see:

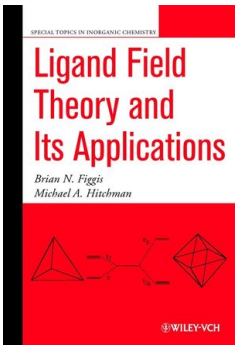

(a) Figgis and Hitchman, Ligand-Field Theory.

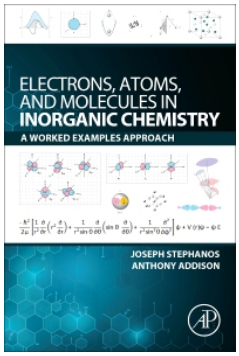

(b) Stephanos and Addison, Electrons in Atoms and Molecules in Inorganic Chemistry.

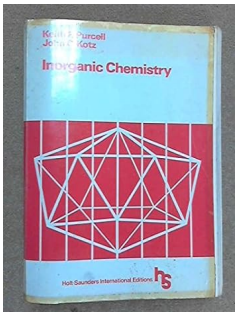

(c) Purcell and Kotz, Inorganic Chemistry.

The spectra that appear regularly in finals papers come from Purcell and Kotz: Inorganic Chemistry:

1.1 Absorption of electromagnetic radiation

The basic features of spectroscopy can be understood in terms of the Beer-Lambert law, which relates the intensities of incident and transmitted radiation. This expression is valid at low concentrations.

The Beer-Lambert law:

$$A = log_{10}\frac{I_0}{I} = \epsilon \cdot c \cdot l \tag{1.1.1}$$

I_0 the intensity of incident light
I the intensity of transmitted light
ϵ *molar absorbtivity* (*extinction coefficient*)
c the concentration of the solution
l the length of the cell

$$f = 4.315 \times 10^{-9} \int \epsilon d\nu \tag{1.1.2}$$

f is the *integrated intensity* or *oscillator strength*

Plot absorbance against wavelength λ (nm) or wavenumber ν (cm^{-1})

ν = number of wavelengths in 1 cm

λ (unit: nm) = 10^7/ν (unit: cm^{-1})

For ν = 10,000 cm^{-1}, λ = 1,000 nm

8067 cm^{-1} = 1 eV = 96.5 kJ mol^{-1}

kT = 200 cm^{-1} at 298 K

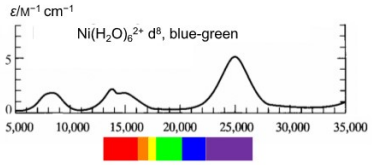

Colour	Wavelength (λ)	Wavenumber (ν)
violet	380 – 450 nm	26,500 – 22,000 cm^{-1}
blue	450 – 495 nm	22,000 – 20,000 cm^{-1}
green	495 – 570 nm	20,000 – 17,500 cm^{-1}
yellow	570 – 590 nm	17,500 – 17,000 cm^{-1}
orange	590 – 620 nm	17,000 – 16,000 cm^{-1}
red	620 – 750 nm	16,000 – 13,000 cm^{-1}
Near infrared	750 – 1,400 nm	13,000 – 7,000 cm^{-1}

(a) Colours and the electromagnetic spectrum

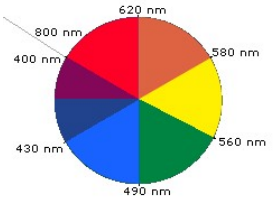

(b) The colour wheel

Figure 1.2: The electromagnetic spectrum and the colour wheel.

1.2 Classes of transitions

We can categorise electronic transitions in transition metal complexes in terms of the nature of the donor and acceptor orbitals. The distinctions can sometimes get blurred when the M-L bonds are very covalent, leading to mixing of metal and ligand character in each orbital. In any given complex, many of the different types of transition may be present but do not lie in the visible region - this doesn't mean they are not happening, just that we can't detect them with the naked eye, and need an appropriate spectrometer!

1. $d \rightarrow d$ transitions occur in open-shell d^n complexes ($n = 1 - 9$). They give information about ligand-field splitting (Δ) and electron-electron repulsion (Racah parameter, B)
2. Ligand-to-metal charge transfer (LMCT). This occurs in all complexes (albeit not always into d orbitals, but often lies outside the visible region
3. Metal-to-ligand charge transfer (MLCT). For this to occur in the visible region, ligands with low-lying π^* orbitals (CO, bipy, phen) are required.
4. Ligand-based (L $\rightarrow$ L). This is typically the domain of organic spectroscopy!
5. $f \rightarrow f$ and $f \rightarrow d$ transitions (in lanthanides/actinides)

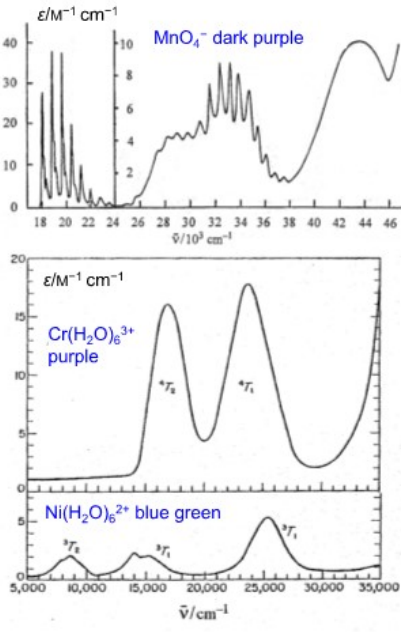

(a) Spectra of $[MnO_4]^-$, $[Cr(H_2O)_6]^{3+}$ and $[Ni(H_2O)_6]^{2+}$.

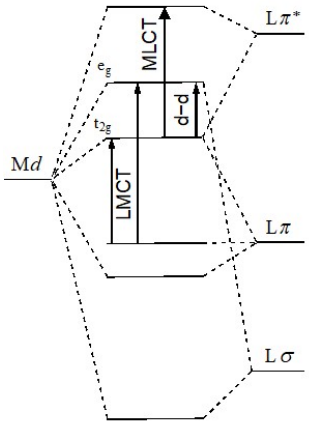

(b) Classes of transitions

Figure 1.3: Representative spectra of transition metal complexes.

1.3 Intensities and selection rules (a brief introduction)

For an electric-dipole allowed transition, the interaction between states of the molecule and electromagnetic radiation is given by the electric dipole moment:

$$Q = \int \psi_f \hat{\mu} \psi_i d\tau = -e \int \psi_f r \psi_i d\tau \tag{1.3.1}$$

$$f \propto Q^2 \tag{1.3.2}$$

$\hat{\mu}$ is the electric dipole moment operator, f is the integrated intensity. If $Q = 0$, the transition is **forbidden**. Otherwise, it is **allowed**. We can make use of group theory to establish when $Q = 0$ (of which much more later), but group theory cannot tell us how big Q is if it is not zero.

1.4 Strong and weak fields

In trying to understand electronic spectra or indeed many other properties of transition metal (or lanthanide) complexes, it is convenient to start from a set of d (or f) orbitals on the metal and add on extra effects such as the ligand field, the repulsion between electrons and spin-orbit coupling. We can also add in even smaller effects like magnetic fields. Mathematically, we would typically do this using **perturbation theory**, the basis of which is that we solve the somewhat simpler problem of the system without the perturbation, and then use the solutions to that simplified problem to find approximate solutions to the system with the perturbation 'switched on'. In the event that there are several perturbations to consider, we would typically deal with the largest first. The distinction between strong and weak-field approaches to transition metal electronic structure lies in the order in which we treat the ligand-field and the electron-electron repulsions. In the $4d$ and $5d$ transition metal elements, the ligand field is typically much larger than the electron-electron repulsion (see Table 1.1), so it makes sense to treat the ligand field first (the 'strong field' approach). In lanthanides, the ligand field is very small because the f orbitals are core-like, so it makes sense to treat electron-electron repulsion and spin-orbit coupling first, and then (maybe) consider the ligand field - the 'weak field' limit. In first-row transition metals, the ligand field and the electron-electron repulsions are of similar magnitude, and in some cases it is convenient to use the strong-field approach, in others the weak field. The truth always lies somewhere between the two limits, and, at least in principle, we should arrive at the same answer whichever limit we start from.

Table 1.1: Ball-park magnitudes of various terms in the Hamiltonian for transition metal and lanthanide complexes.

		1st row TM	**2nd row TM**	**lanthanide**
d **orbitals**	**ligand field**	10000 cm^{-1}	20000 cm^{-1}	1-10 cm^{-1}
	e-e repulsions	10000 cm^{-1}	2000 cm^{-1}	5000-10000 cm^{-1}
	spin-orbit coupling	100-1000 cm^{-1}	1000-2000 cm^{-1}	500-3000 cm^{-1}

1.5 Spectra of ions with d^1, d^4, d^6 and d^9 configurations

1.5.1 Strong-field limit

The spectra of complexes with these configurations are particularly simple - they feature a single transition (albeit sometimes split, as we shall see later). For d^1, the reasons are quite obvious - there is only one electron, therefore no electron-electron repulsion to worry about. Our starting point for interpreting the spectra is therefore a set of d orbitals, split into t_{2g} and e_g sets by the ligand field. For the others, the situation is less clear, but by either (1) noting that a filled shell of spin-α electrons is totally symmetric or (2) treating holes in the d shell in the same way as electrons, we can treat d^4, d^6 and d^9 in the same way.

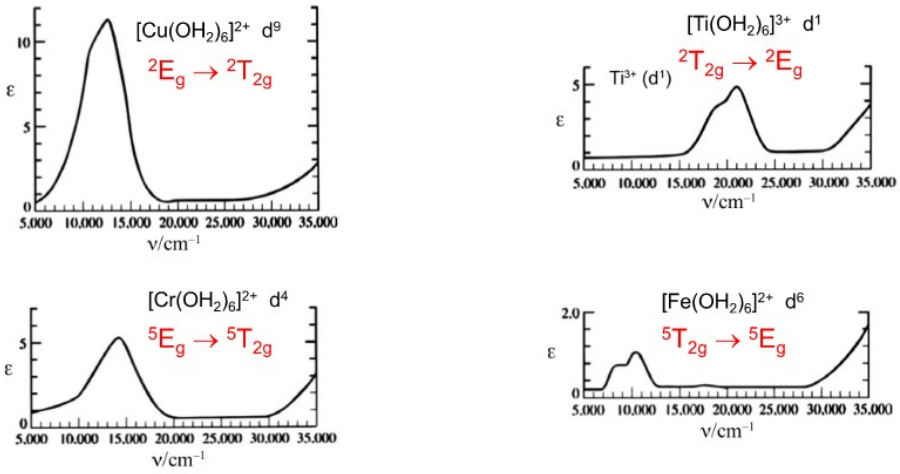

Figure 1.4: Spectra of d^1, d^4, d^6 and d^9 transition metal complexes

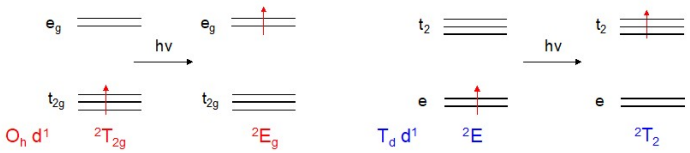

Figure 1.5: $d \rightarrow d$ transitions in octahedral and tetrahedral d^1 systems

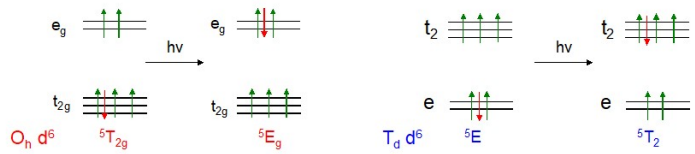

Figure 1.6: $d \rightarrow d$ transitions in octahedral and tetrahedral d^6 systems

Note that the five spin-α electrons fill the d shell as symmetrically as possible - this means that

the symmetry of the state is determined solely by the symmetry of the orbital containing the single spin-β electron.

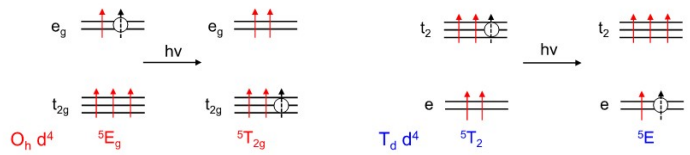

Figure 1.7: $d \rightarrow d$ transitions in octahedral and tetrahedral d^4 systems

The single 'hole' in the spin-α set has the same symmetry properties as a single electron (d^1), except that 'holes' prefer to be in high-energy orbitals while electrons prefer to be in low-energy ones. The ground-state therefore has the hole in the upper e_g orbital, and has ${}^5E_g$ symmetry.

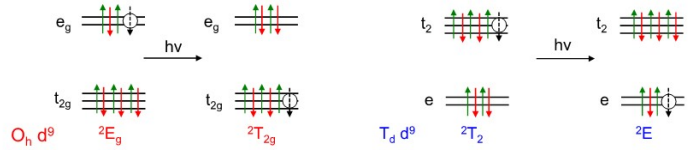

Figure 1.8: $d \rightarrow d$ transitions in octahedral and tetrahedral d^9 systems

The single 'hole' in the spin-β set has the same symmetry properties as a single spin-β electron in d^6, with the same caveat that 'holes' prefer to be in high-energy orbitals. The ground-state therefore has the hole in the upper e_g orbital, and has ${}^2E_g$ symmetry while the excited state has ${}^2T_{2g}$ symmetry.

1.5.2 Weak-field limit

Let us now look at the same problem from the weak-field perspective. We start here by generating the states of the free ion, then considering how they split in octahedral symmetry. The first step is rather trivial as there is only 1 electron, but it is useful to set out the process before we see it again in more complex multi-electron cases. The total degeneracy is 10 (10 choices of box to put the electron) with a ground state of ^2D, obtained by summing m_l to get L and summing m_s to get S.

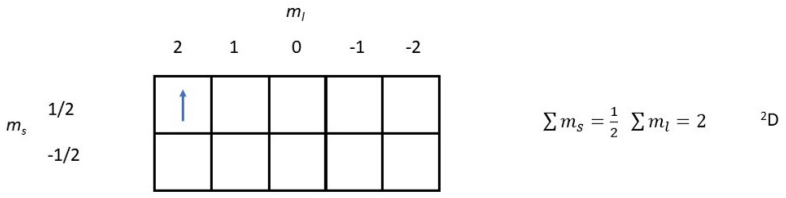

Figure 1.9: Atomic ground state for a d^1 system.

The variation in energy of the $^2T_{2g}$ and ^2E_g states as a function of the ligand-field splitting diagram is shown on the right hand side of the ***Orgel diagram*** shown in Figure 1.10. The free atom/ion is placed in the centre, and the splitting of levels is shown to right: the $T_{2(g)}$ state falls below $E_{(g)}$ as Δ increases. We can also use the right-hand side of the diagram for octahedral d^1 and d^6 as well as for tetrahedral d^4 and d^9: in all cases, the ground state has $^2T_{2g}$ symmetry. The splitting to the left, where the $E_{(g)}$ state lies below $T_{2(g)}$, is appropriate for octahedral d^4 and d^9 as well as tetrahedral d^1 and d^6. In all cases, the splitting is exactly equal to $\Delta_{o/t}$.

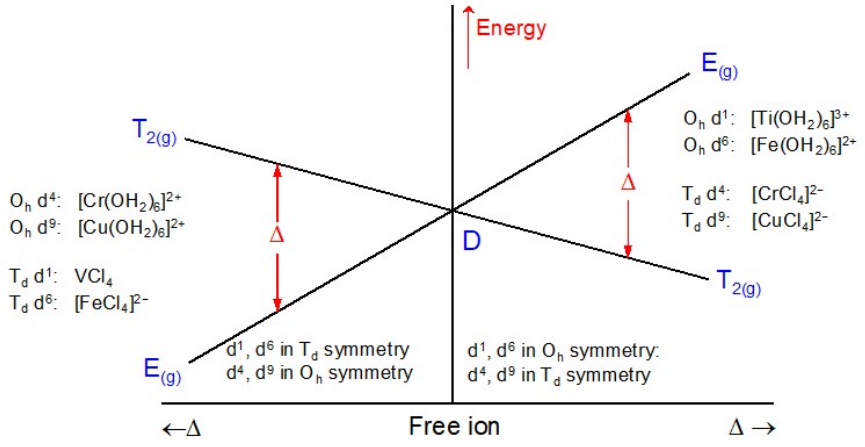

Figure 1.10: Orgel diagram for d^1, d^4,d^6 and d^9

1.5.3 Jahn-Teller distortions in $[Ti(H_2O)_6]^{3+}$ and $[Cu(H_2O)_6]^{2+}$

The Jahn-Teller theorem states that *a non-linear molecule in an orbitally degenerate state will distort so as to remove the degeneracy.*[1] States with E_g and T_{2g} symmetry are orbitally degenerate, so in both cases the molecule should distort spontaneously away from the octahedron. In the ground state, the effects on structure are very clear and well-known in *e.g.* $[Cu(H_2O)_6]^{2+}$ and $[Cr(H_2O)_6]^{2+}$, where the unpaired electron is in the e_g orbital and the axial bond lengths are typically much longer than their equatorial counterparts. The structural consequences of the Jahn-Teller theorem are much less obvious when the degeneracy lies in the t_{2g} orbitals, and indeed the geometries of $[Ti(H_2O)_6]^{3+}$ and $[Fe(H_2O)_6]^{2+}$ are close to perfectly octahedral. The E_g and T_{2g} states behave different because whilst the e_g orbitals interact very strongly with the ligands (they are M-L σ antibonding), the t_{2g} orbitals do not (they are π bonding/antibonding). As a result, different distributions of electrons amongst the degenerate orbitals have much less impact on metal-ligand bond lengths in T states.

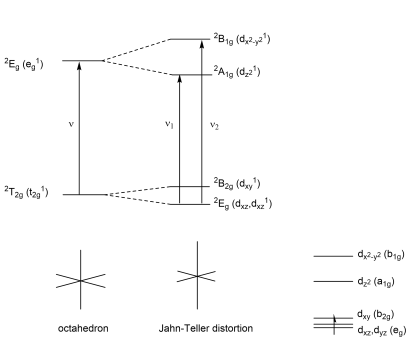

(a) Spectrum of $[Ti(H_2O)_6]^{3+}$

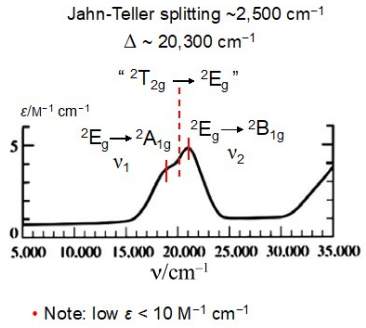

(b) State splitting in $[Ti(H_2O)_6]^{3+}$

Figure 1.11: Influence of Jahn-Teller splitting in $[Ti(H_2O)_6]^{3+}$

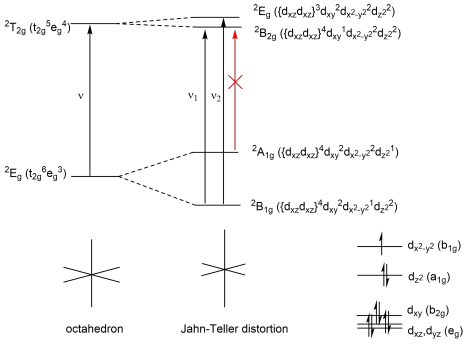

(a) Spectrum of $[Cu(H_2O)_6]^{2+}$

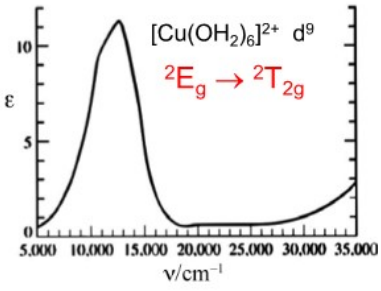

(b) State splitting in $[Cu(H_2O)_6]^{2+}$

Figure 1.12: Influence of Jahn-Teller splitting in $[Cu(H_2O)_6]^{2+}$

Despite their near-perfect ocahedral structures, it is clear that the splitting of the $d \rightarrow d$ bands in

[1] note that the theorem is definitive: the molecule will distort. It does not, however, specify how it will distort, or how much it will distort: it is quite possible that the distortion is there, but is too small to detect using typical experimental techniques.

Figure 1.4 is most prominent for $[Ti(H_2O)_6]^{3+}$ and $[Fe(H_2O)_6]^{2+}$ - *i.e.* systems where the ground state has T_{2g} symmetry amd the excited states is E_g. In the state-splitting diagram for $[Ti(H_2O)_6]^{3+}$ in Figure 1.11a, the ground $^2T_{2g}$ state is split by ≈ 400 cm^{-1} while the ^2E_g excited state is split by ≈ 2500 cm^{-1}, and the result is that the transition is split into two components separated by ≈ 2500 cm^{-1}. In $[Cu(H_2O)_6]^{2+}$ in Figure 1.12a, the large splitting is in the ground state, only the lower component of which ($^2B_{1g}$) is populated at ambient temperature. As a result, we see only transitions from $^2B_{1g}$ to the components of the excited $^2T_{2g}$ state, which are split by a much smaller amount. In electronic spectroscopy, we see the impact of the Jahn-Teller effect only if it is significant in the *excited state*, not the ground state, whereas in crystallography it is the opposite.

1.6 Intensities and selection rules: detailed treatment

It is often stated that '$d \rightarrow d$ transitions are forbidden'. What does 'forbidden' mean, and why do all transition metal complexes still have some colour (albeit sometimes very weak) if all the transitions are forbidden? The intensity of '$d \rightarrow d$ transitions' depends strongly on the metal in question, the symmetry of the complex and the type of ligands, so clearly 'forbidden' is only a starting point.

1. $d \rightarrow d$ transitions in octahedral complexes typically have $\epsilon < 10$ M^{-1}cm^{-1}
2. $d \rightarrow d$ transitions in tetrahedral complexes typically have ϵ between 10 M^{-1}cm^{-1} and 1000 M^{-1}cm^{-1}

$$Q = \int \psi_f \hat{\mu} \psi_i d\tau = -e \int \psi_f r \psi_i d\tau \tag{1.6.1}$$

$\hat{\mu} = -er$ is the dipole moment operator. It transforms in the same way as x, y, z, so as T_{1u} in O_h symmetry, T_2 in T_d symmetry *etc.*

For $Q > 0$, the following condition must apply: $\Gamma(\Psi_f) \otimes \Gamma(\hat{\mu}) \otimes \Gamma(\Psi_i)$ must contain the totally symmetric representation.

When analysing intensities, always break the problem down into two separate questions:

1. Is $Q = 0$? Group theory can be used to answer this.
2. If $Q \neq 0$, how big is Q? Here, we either have to evaluate the integral Q (difficult!), or make qualitative arguments about its likely magnitude.

1.6.1 Spin selection rule

If we ignore spin-orbit coupling, we can separate the spin and spatial parts of the electronic wavefunction:

$$\psi^{elec} = \psi^{spatial} \times \psi^{spin} \tag{1.6.2}$$

and so, because the dipole moment operator does not act on the spin part:

$$Q = \int \psi_f \hat{\mu} \psi_i d\tau = \int \psi_f^{spatial} \hat{\mu} \psi_i^{spatial} d\tau \times \int \psi_f^{spin} \psi_i^{spin} d\tau \tag{1.6.3}$$

So for $Q \neq 0$, we need 2 conditions to be met:

$$\int \psi_f^{spatial} \hat{\mu} \psi_i^{spatial} d\tau \neq 0 \tag{1.6.4}$$

$$\int \psi_f^{spin} \psi_i^{spin} d\tau \neq 0 \tag{1.6.5}$$

The second of these is the basis of the spin selection rule: $Q = 0$ only if $\Delta S = 0$. This selection rule breaks down if spin-orbit coupling is significant, in which case our initial assumption of separability of the wavefunction breaks down. However, in almost all cases we will be concerned with, the spin selection rule is a good one, and all intense transitions will be spin-allowed.

1.6.2 Orbital selection rules: the Laporte and parity selection rules

We can usefully start our analysis of this term by considering the case of atoms (with spherical symmetry), where the Laporte selection rule tells us that allowed transitions (*i.e.* those with $Q \neq 0$) have $\Delta l = \pm 1$. So, in atoms:

1. all $s \rightarrow p$, $p \rightarrow d$, $d \rightarrow f$ transitions are allowed
2. all $s \rightarrow s$, $p \rightarrow p$, $d \rightarrow d$, $f \rightarrow f$, $s \rightarrow d$, $p \rightarrow f$ transitions are forbidden

It is often stated that *'d-d' transitions are also forbidden in metal complexes* but how/why are we entitled to even think about d orbitals existing in complexes: 'd' (along with 's', 'p' and 'f'), are labels of the irreducible representations of R_3, the full rotation group – strictly speaking, such labels have no business being any where near a complex with finite symmetry! But, as long as the perturbation of the metal atom/ion is sufficiently weak, the wavefunction retains sufficient 'memory' of being a d orbital that this remains a useful starting point. However, it is important to remember that to describe an orbitals as a 'd orbital' in a metal complex is always an approximation, and the extent to which this approximation is a good one is the key to understanding intensities.

Octahedral complexes. Consider a $t_{2g} \rightarrow e_g$ transition in an octahedral d^1 complex.

$\Gamma(\Psi_i) = T_{2g}$, $\Gamma(\Psi_f) = E_g$, $\Gamma(\hat{\mu}) = T_{1u}$

Using the direct product table and also $g \otimes g = g$, $u \otimes u = g$, $g \otimes u = u$:

$$\Gamma(\Psi_f) \otimes \Gamma(\hat{\mu}) \otimes \Gamma(\Psi_i) = E_g \otimes T_{1u} \otimes T_{2g} = (T_{1u} + T_{2u}) \otimes T_{2g} = A_{1u} + A_{2u} + 2E_u + 2T_{1u} + 2T_{2u}$$

Clearly this does not contain the totally symmetric representation, so the transition is forbidden. We could have saved ourselves some work in evaluating the triple product above by noting that for $E_g \otimes T_{1u} \otimes T_{2g}$ to contain A_{1g}, it is necessary that $E_g \otimes T_{2g}$ must contain T_{1u}. From the direct product table, $E_g \otimes T_{2g} = T_{1g} + T_{2g}$, so again we can confirm that the transition is forbidden. We could save even more time by noting that $g \otimes u = u$, so all the components of the triple product must be u, and it therefore cannot possibly contain A_{1g}. In general, in centrosymmetric groups, $\Gamma(\hat{\mu})$ will always have ungerade symmetry, so the direct product $\Gamma(\Psi_f) \otimes \Gamma(\Psi_i)$ must have ungerade symmetry if the condition for $Q \neq 0$ is to be met. This leads to the **parity selection rule**: $g \rightarrow u$

Table 1.2: Direct products for the T_d, T, O_h and O point groups.

	A_1	A_2	E	T_1	T_2
A_1	A_1	A_2	E	T_1	T_2
A_2		A_1	E	T_2	T_1
E			$A_1 + [A_2] + E$	$T_1 + T_2$	$T_1 + T_2$
T_1				$A_1 + E + [T_1] + T_2$	$A_2 + E + T_1 + T_2$
T_2					$A_1 + E + [T_1] + T_2$

is allowed but $g \rightarrow g$ and $u \rightarrow u$ are forbidden. We can connect the parity and Laporte selection rules by noting the following (using the octahedral character table, Table 1.3):

Table 1.3: Character Table for O_h

O_h	E	$8C_3$	$6C_2$	$6C_4$	$3C_2$	i	$6S_4$	$8S_6$	$3\sigma_h$	$6\sigma_d$		
A_{1g}	1	1	1	1	1	1	1	1	1	1		$x^2 + y^2 + z^2$
A_{2g}	1	1	-1	-1	1	1	-1	1	1	-1		
E_g	2	-1	0	0	2	2	0	-1	2	0		$(2z^2 - x^2 - y^2,\, x^2 - y^2)$
T_{1g}	3	0	-1	1	-1	3	1	0	-1	-1	(R_x, R_y, R_z)	
T_{2g}	3	0	1	-1	-1	3	-1	0	-1	1		$(xy,\, xz,\, yz)$
A_{1u}	1	1	1	1	1	-1	-1	-1	-1	-1		
A_{2u}	1	1	-1	-1	1	-1	1	-1	-1	1		
E_u	2	-1	0	0	2	-2	0	1	-2	0		
T_{1u}	3	0	–1	1	–1	-3	-1	0	1	1	(x, y, z)	
T_{2u}	3	0	1	-1	–1	-3	1	0	1	-1		

1. t_{2g} orbitals have exclusively d character (d_{xz} d_{yz}, d_{xy})
2. e_g orbitals have exclusively d character (d_{z^2}, $d_{x^2-y^2}$)
3. t_{1u} orbitals have p character (p_x, p_y, p_z)
4. a_{1g} orbitals have s character

$\therefore$ there is **no** mixing of d character with p or s.

So, when we describe the $t_{2g} \rightarrow e_g$ transition in *e.g.* $[\mathrm{Ti(OH_2)_6}]^{3+}$ as a '$d \rightarrow d$ transition', this is a good approximation because the orbitals involved have no s, p or f character on the metal (although they do, of course, have some ligand character). The symmetry is therefore high enough that these transitions "retain the memory" of their '$d \rightarrow d$' origins, and the intensity remains low. The parity selection rule is sometimes considered as a subsidiary of the Laporte rule: the rule that $g \rightarrow g$ is

forbidden effectively captures all the $d \rightarrow d$ ($\Delta l = 0$) and $s \rightarrow d$ ($\Delta l = 2$) transitions that were forbidden by Laporte. Given the forbidden nature of these transitions, it is valid to ask why we see any intensity at all in octahedral complexes. We return to this question in Section 1.6.2, but it is useful first to consider the family of tetrahedral complexes.

Tetrahedral complexes. General observation: the intensity of '$d \rightarrow d$' transitions in tetrahedral complexes is up to an order of magnitude higher than octahedral complexes. The intensity is also dependent on ligand, with more covalent ligands (Br^-, for example) giving greater intensity than more 'ionic' ones (F^-, for example). There is a simple but superficial answer to this question based on group theory:

For a d^1 complex in tetrahedral symmetry (ground state configuration $e^1t_2^0$):

$\Gamma(\Psi_i) = E$, $\Gamma(\Psi_f) = T_2$, $\Gamma(\hat{\mu}) = T_2$

$\Gamma(\Psi_f) \otimes \Gamma(\hat{\mu}) \otimes \Gamma(\Psi_i) = E \otimes T_1 \otimes T_2 = A_1 + A_2 + 2E + 2T_1 + 2T_2$

which **does** contain the totally symmetric representation, A_1, and so the transition is allowed from a group theoretical perspective. The key difference compared to the octahedron is that there is no centre of symmetry, therefore no g and u labels, therefore no parity selection rule to worry about. However, remember that the selections rules tell us only whether $Q = 0$ or not - they tell us nothing about how large Q is in the event that it is not zero. So all we have established at this stage is that the intensity should be zero in an octahedron, and not zero in a tetrahedron.

Thought experiment: what would happen if the metal-ligand bond lengths in the tetrahedron were 1 m, or 1 km? The complex is no less tetrahedral as a result, but common sense suggests that the $d \rightarrow d$ transition should revert smoothly back to its 'atomic' character - *i.e.* forbidden - as we elongate the bonds to infinity. So we need a more nuanced picture which takes into account not just the gross symmetry, but also the extent to which the ligand arrangement perturbs the electronic structure of the metal orbitals.

From the T_d character table:

T_d	E	$8C_3$	$3C_2$	$6S_4$	$6\sigma_d$		
A_1	1	1	1	1	1		$x^2 + y^2 + z^2$
A_2	1	1	1	–1	–1		
E	2	–1	2	0	0		$(2z^2 - x^2 - y^2,\ x^2 - y^2)$
T_1	3	0	–1	1	–1	(R_x, R_y, R_z)	
T_2	3	0	–1	–1	1	(x, y, z)	$(xy,\ xz,\ yz)$

1. t_2 orbitals now have **both** d and p character (d_{xz}, d_{yz}, d_{xy}, p_x, p_y, p_z)

2. e orbitals still have exclusively d character (d_{z^2}, $d_{x^2-y^2}$)

So now when, when we describe the $e \rightarrow t_2$ transition in *e.g* $[CoCl_4]^{2-}$ as a '$d \rightarrow d$' transition, this is not such a good approximation any more – it is really a '$d \rightarrow d$ plus a bit of $d \rightarrow p$' transition, and it is the $d \rightarrow p$ part that raises the intensity. The absence of parity admits the possibility that d and p can mix, and this, in turn, admits the possibility that the $e \rightarrow t_2$ transition will gain intensity by virtue of its partial $d \rightarrow p$ character. The critical piece of information needed to understand the intensities is therefore *how much* p character is mixed into the 'mostly' d orbital.

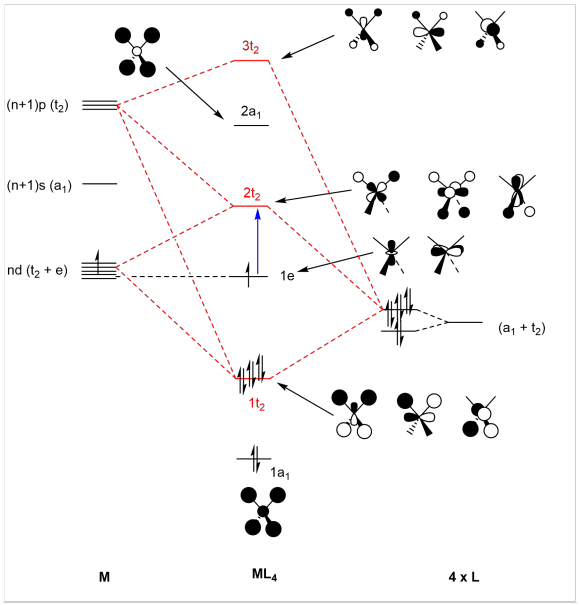

Figure 1.13: MO diagram for a tetrahedral complex.

The essential requirement for effective mixing of p and d orbitals on a metal is that there must be an orbital on the ligands that can interact effectively with **both** p and d.[2] Interacting with only one or the other is not enough - it has to be both.

Effective interaction can only be achieved if:

1. the ligand orbital is high enough in energy that $\frac{1}{\Delta E}$ is not too small to either d or p and
2. the ligand-based orbital must overlap effectively with **both** p and d.

In general, more 'covalent' ligands meet the the first criterion better, so Br^- will induce more $d-p$ mixing in t_2, and hence more intensity into the $e \rightarrow t_2$ transition. The second criterion will be met when the sizes of the nd and $(n+1)p$ orbitals are not too different.[3]

[2] In the absence of ligands, p and d are strictly orthogonal - they do not mix

[3] Similar factors are relevant to $s-p$ hybridisation in main group molecules - effective $s-p$ hybridisation occurs only when a ligand overlaps with both s and p. When the s orbital become very contracted relative to p, we lose $s-p$ hybridisation - this is the '*inert-pair effect*'.

Vibronic coupling in octahedral complexes. In section 1.6.2 we noted that '$d \rightarrow d$' transitions were group-theoretically forbidden due to the parity selection rule, and that this forbidden-ness could be traced to fact that the orbitals largely retain their atomic identity even in the complex, ensuring that there is no $d-p$ mixing of the type found in tetrahedra. So why, then, do we see any intensity at all in the $d \rightarrow d$ transitions?

The fundamental M-L stretching modes of the octahedron are shown in Figure 1.14a: they span $A_{1g} + E_g + T_{1u}$. When the T_{1u} mode is excited, the molecule is no longer O_h-symmetric - rather it has the lower C_{4v} symmetry where there is no centre of symmetry and so all the arguments we made about $d-p$ mixing for the T_d point group become relevant. This is known as '**vibronic coupling**'. We see from the C_{4v} character table that d_{xz} and d_{yz} transform as E, as do p_x and p_y, while d_{z^2} and p_z both transform as A_1. d_{xy} and $d_{x^2-y^2}$ transform as B_2 and B_1, respectively, and remain pure 'd.' So at least some of the '$d \rightarrow d$ transitions' are really a '$d \rightarrow d$ plus a bit of $d \rightarrow p$' transition. Note that the a_g and e_g-symmetric vibrational modes do not remove the centre of symmetry, so do not induce $d-p$ mixing.

In this light, we see that the essential difference between octahedral and tetrahedral complexes is that $d-p$ mixing is **always** allowed in the latter, but in the former it only comes into play if the molecule is excited into specific vibrational modes.

If it is excited into the T_{1u} mode, we then need to consider the extent to which the vibrations actually induce meaningful mixing - if the bonds are very ionic (or 1 km long!), vibrations won't actually mix d and p to any great extent, even though they can from a purely group theoretical perspective, and the intensity will remain low. The result is that vibronic coupling is much more effective for covalent ('soft') rather than ionic ('hard') ligands. Vibronic coupling also becomes more efficient as the amplitude of the vibration increases (affording more effective overlap with the metal d orbitals), so the intensity of vibronically-allowed transitions tends to increase with temperature (Figure 1.15). In a tetrahedron (or any non-centrosymmetric group such as D_{2d}), in contrast, $d-p$ mixing occurs irrespective of whether the molecule is vibrating or not, so the intensities are much less dependent on temperature.

Table 1.4: Character Table for C_{4v}

C_{4v}	E	$2C_4$	C_2	$2\sigma_v$	$2\sigma_d$		
A_1	1	1	1	1	1	z	z^2,x^2+y^2
A_2	1	1	1	-1	–1		
B_1	1	–1	1	1	-1		x^2-y^2
B_2	1	–1	1	–1	1		xy
E	2	0	–2	0	0	(x,y)	(xz,yz)

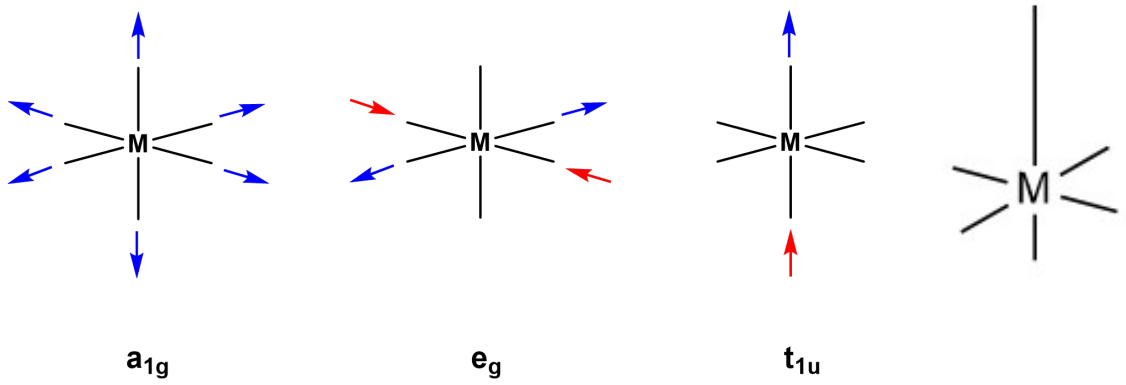

(a) M-L stretching modes of an octahedron

Figure 1.14: Vibronic coupling in an octahedron

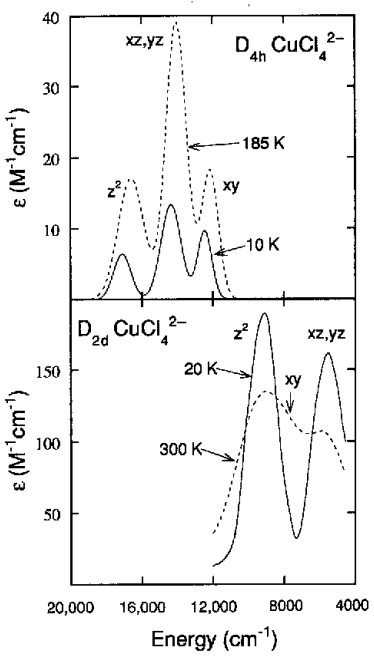

Figure 1.15: Temperature dependence of the vibronically-allowed bands in D_{4h}- and D_{2d}-symmetric isomers of $[CuCl_4]^{2-}$. Note (a) that at low temperature the intensities of the bands in centrosymmetric D_{4h} are an order of magnitude smaller and (b) that the intensities of the vibronically allowed bands of the centrosymmetric complex are temperature dependent while those of the non-centrosymmetric complex (which do not rely on vibronic coupling for their intensity) are not.

A more rigorous group theoretical approach to vibronic coupling. We have thus far focussed on the electronic wavefunction, ψ^{elec}, but the total wavefunction, ψ, is the product of

electronic and vibrational parts: $\psi = \psi^{elec} \cdot \psi^{vib}$. The ground-state vibrational wavefunction is always the totally symmetric representation of the relevant point group, so if we are concerned only with ground state, the symmetry of the ψ is that same as that of ψ^{elec} (which is why we don't usually worry about the vibrational part!). We can then recast the expression for the dipole moment, Q, as:

$$Q = \int \psi_f \hat{\mu} \psi_i d\tau = \int \psi_f^{elec} \psi_f^{vib} \, \hat{\mu} \, \psi_i^{elec} \psi_i^{vib} d\tau \tag{1.6.6}$$

The condition for $Q \neq 0$ is then:

$$\Gamma(\psi_f^{elec}) \otimes \Gamma(\psi_f^{vib}) \otimes \Gamma(\hat{\mu}) \otimes \Gamma(\psi_i^{elec}) \otimes \Gamma(\psi_i^{vib}) \tag{1.6.7}$$

must contain the totally-symmetric representation. For a d^1 $t_{2g} \rightarrow e_g$ transition, this gives:

$$E_g \otimes \Gamma(\psi_f^{vib}) \otimes T_{1u} \otimes T_{2g} \otimes A_{1g} \tag{1.6.8}$$

so $\Gamma(\psi_f^{vib})$ must match one of the components of the direct product $E_g \otimes T_{1u} \otimes T_{2g} \otimes A_{1g}$. We could work this quadruple product out with the direct product tables, but it is clear that every component will have 'u' symmetry because only one component of the quadruple product has 'u' symmetry and $g \otimes u \otimes g \otimes g = u$. Therefore $\Gamma(\psi_f^{vib})$ **must** be 'u' to make the overall product symmetric ('g'). This is what we anticipated from the simple arguments about loss of the center of symmetry above.

Vibronic coupling and bandwidths A complementary aspect of vibronic coupling is that it broadens bands. Again, there is a simple explanation and a more nuanced one. The simple explanation is that during a vibration, the ligands are closer/further away from the metal, and so the ligand-field splitting, Δ, is different at each point. So depending on where the complex is on the vibrational potential energy surface when it is excited (note that excitation is instantaneous), Δ will take on a range of values and hence the single excitation energy of the static complex will take on a range of values.

So why are some bands in MnF_2 broad (the $^4T_{1g}$ band at 19000 cm^{-1}, for example) but some are sharp (the ^4E_g band at 25000 cm^{-1}). This, again, depends on the extent to which the vibrations of the ligand are coupled to the orbitals on the metal. The 'ligand-field' transitions in Figure 1.16c ($^6A_{1g} \rightarrow^4 T_{1g}$, for example) involve a change in population of the M-L σ antibonding e_g orbitals, so the bonds will be longer in the excited state. Conversely, 'spin-flip' transitions ($^6A_{1g} \rightarrow^4 E_g$, for example) do not change the population of the e_g orbitals, so the bond lengths in ground and excited states are approximately the same, and we see very limited vibronic coupling. Spin-flip transitions are intrinsically weak, so we only see them in high-spin d^5 complexes, where there are no spin-allowed transitions in the same region.

1.6.3 A brief look at lanthanide spectroscopy

$f \rightarrow f$ transitions can be spin-allowed or spin-forbidden (in the case of f^7). The characteristic behaviour of f orbitals is that they are core-like, which makes the effects of vibronic coupling very small. As a result, their spectra show weak $f \rightarrow f$ transitions that are not broadened by the Frank-Condon factor (in that sense they are very like the spin-flip transitions in Mn^{2+}). However, spin-orbit coupling is larger in the lanthanides than the first-row transition metals, which relaxes

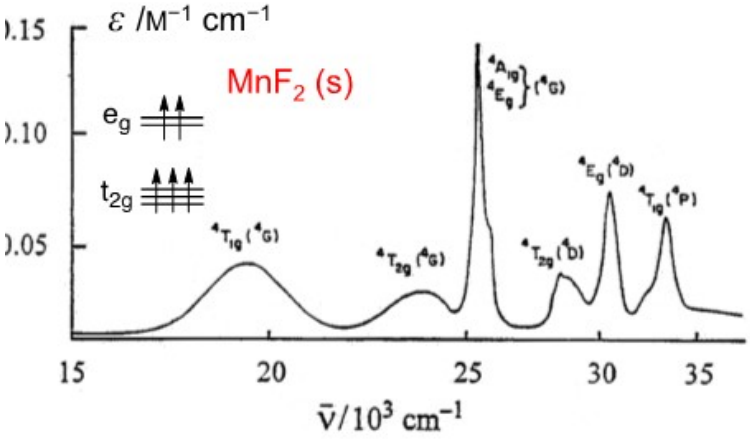

(a) Spectrum for a high-spin d^5 complex.

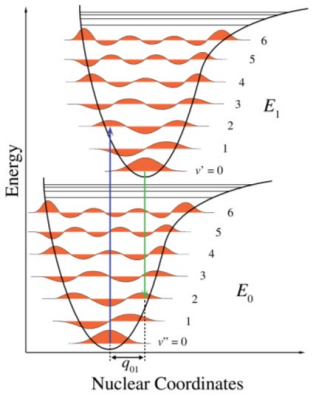

(b) Frank-Condon overlap for ligand-field transitions

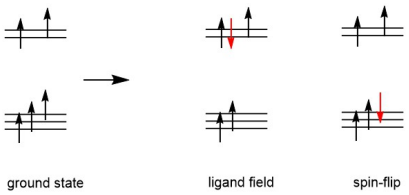

(c) Ligand-field (*e.g.* $^4T_{1g}$) and spin-flip (*e.g.* $^4A_{1g}$) transitions for a high-spin d^5 complex, MnF_2.

Figure 1.16: Impact of vibronic coupling on band widths

the Laporte selection rule as well, in the case of f^7 systems (Eu^{2+}, Gd^{3+}), as the spin selection rule. As a result, the extinction coefficients, ϵ, are typically somewhat larger than those of high-spin d^5 ions such as Mn^{2+}. The absence of significant ligand-field splitting means that spectra are typically labelled according to their atomic state ($^1D_2$ *etc.*) rather than the representations of a finite point group.

1.6.4 Ball-park summary of trends in extinction coefficients

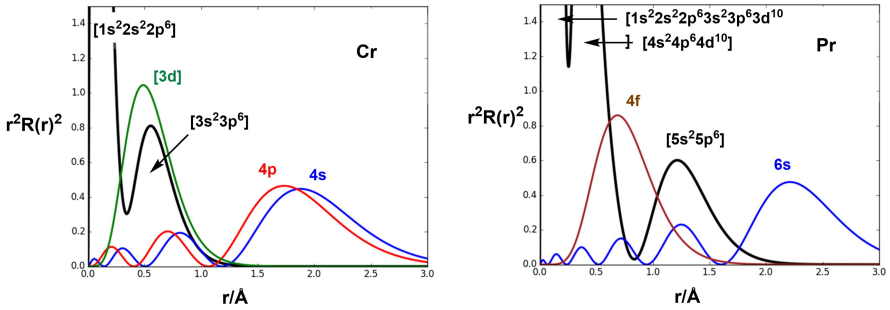

(a) Radial distribution functions for typical transition metal and lanthanide elements.

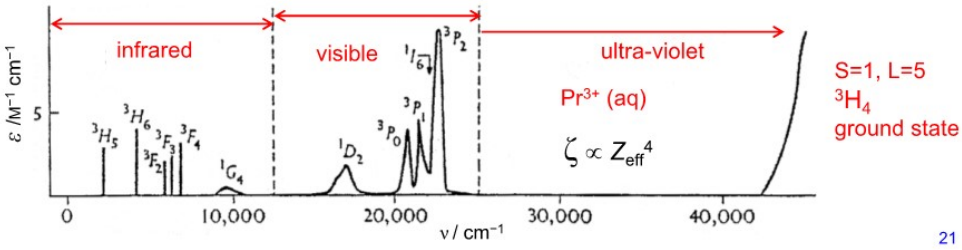

(b) Spectrum of the Pr^{3+} ion.

Table 1.5: Ball-park magnitudes of extinction coefficients in various classes of complex.

Type	Example	Typical ϵ_{max} / $M^{-1}cm^{-1}$
spin-forbidden $d \rightarrow d$	Mn^{2+}	< 0.1
spin-allowed $f \rightarrow f$	Pr^{3+}	1-10
spin-allowed $d \rightarrow d$, centrosymmetric	$[Cr(H_2O)_6]^{3+}$	5-100
spin-allowed $d \rightarrow d$, non-centrosymmetric	$[CoCl_4]^-$	100-800
spin-allowed charge transfer	$[MnO_4]^-$	10^4
spin-allowed ligand $\pi \rightarrow \pi^*$	porphyrins	10^5

1.7 Electronic spectra of complexes with d^2, d^3, d^7 and d^8 configurations.

When more than one electron is present, we need to add electron-electron repulsion to the list of perturbations, along with the ligand field. We need, therefore, to decide which order to include them: ligand-field first (the strong-field limit) or electron-electron repulsion first (the weak-field limit). They should yield the same answer (same number of states, same symmetries, same energies) as long as the various perturbations are applied correctly.

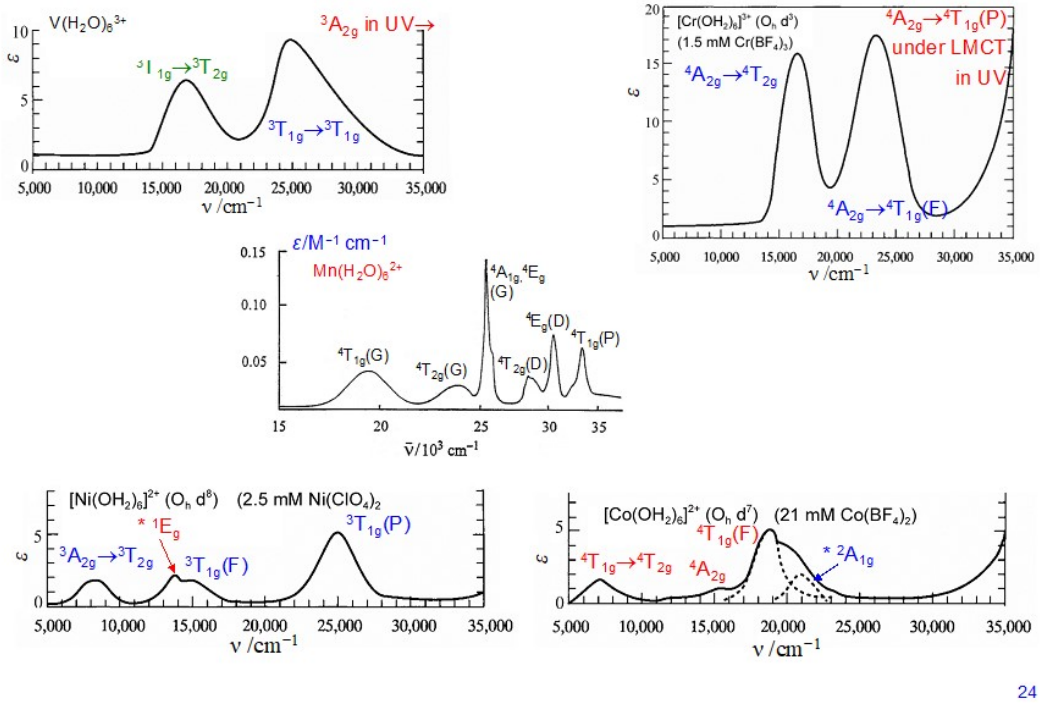

24

Figure 1.18: Electronic spectra of representative complexes with d^2, d^3, high-spin d^5, d^7 and d^8 configurations.

1.7.1 Spectra of d^2 systems: $[\mathbf{V(H_2O)_6}]^{3+}$

Strong-field limit In the strong-field approach we first split the five d orbitals into the familiar t_{2g} and e_g sets, and then identify all of the states that arise from the different arrangements of two electrons in these orbitals. It is useful to keep track of how many states we are looking for. There are $10 \times 9 \div 2 = 45$ ways of arranging 2 electrons in 10 spin orbitals. However, Hund's rule tells us that the ground state will be a triplet and, if we focus only on the $M_S = 1$ components of the triplets, we are restricted to putting the two electrons in the upper $m_s = +\frac{1}{2}$ boxes. We then have $5 \times 4 \div 2 = 10$ states with $M_S = 1$. We must have an equivalent set of 10 for each of $M_S = 0$ and $M_S = -1$, so 30 of the micro-configurations make up the triplets.

For the ground state (t_{2g}^2), the direct-product table, Table 3.10, tells us that the only triplet state is $^3T_{1g}$ (the square bracket identifies the triplet). The $t_{2g}^1 e_g^1$ configuration gives $^3T_{1g}$ and $^3T_{2g}$ (the Pauli principle places no restriction here because we have electrons in different orbitals, so we get triplet and singlets for each spatial component). Finally, the e_g^2 configuration generates $^3A_{2g}$. Taking into account the three-fold degeneracy of the T states, we have 10 states with $M_S = 1$, as we anticipated above.

What differentiates the $^3T_{1g}$ and $^3T_{2g}$ states if they arise from the same $t_{2g}^1 e_g^1$ configuration? In the first case the unpaired electrons are in the d_{xy} component of t_{2g} and the d_{z^2} component of e_g, while in the other they are in d_{xy} and $d_{x^2-y^2}$. The electron-electron repulsions in the two cases

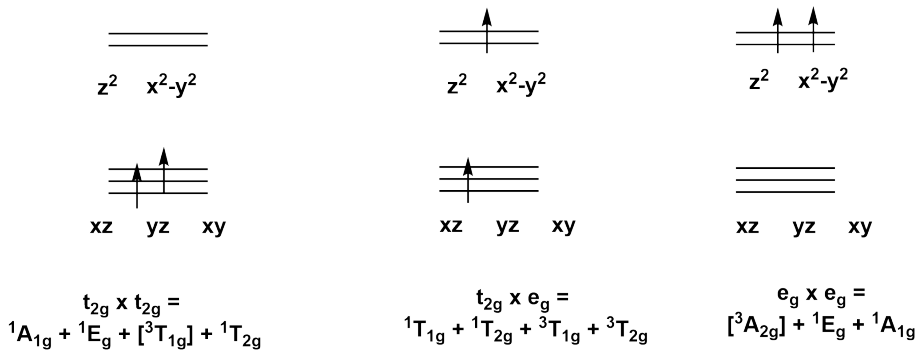

Figure 1.19: d^2 configurations

are therefore different, and so the energies are different. States arising from the same configuration differ in their electron-electron repulsions.

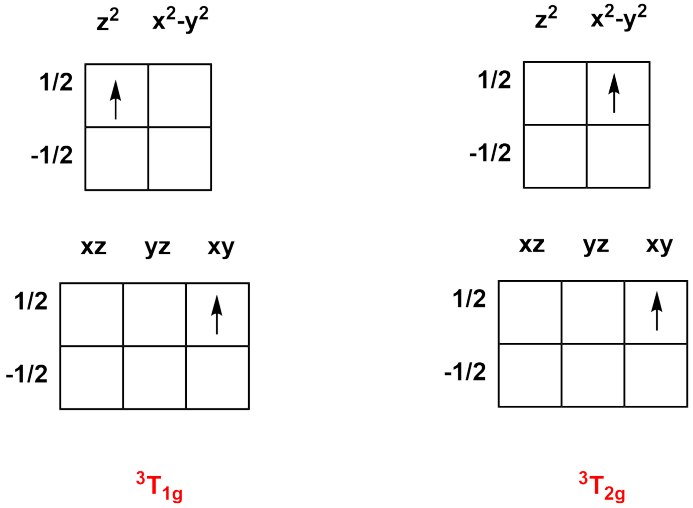

Figure 1.20: Difference between ${}^3T_{1g}$ and ${}^3T_{2g}$ states. Note that each state has three distinct terms: only one of each is shown here.

Weak-field limit Now, let's tackle the same d^2 problem in the reverse order, by considering the electron-electron repulsions first, then adding the ligand field. There are again $10 \times 9 \div 2 = 45$ micro-configurations in total, of which $5 \times 4 \div 2 = 10$ are the $M_S = 1$ components of the triplets. These are shown in Figure 1.21 and we see that they generate two triplets, ${}^3F$ and ${}^3P$. By Hund's second rule, the ${}^3F$ state should be more stable, and the difference between the two is given by $15B$, where B is the *Racah parameter*, a measure of electron-electron repulsion. We can then use descent in symmetry tables to show that in an octahedral field, the ${}^3F$ state splits into ${}^3T_{1g} +^3 T_{2g} +^3 A_{2g}$ while ${}^3P$ remains three-fold degenerate (in both space and spin), ${}^3T_{1g}$.

The states split according to Figure 1.22. Note that the two ${}^3T_{1g}$ states will interact and repel

Table 1.6: Descent in symmetry table from R_3 to O, D_6, D_5, D_4 and D_3

R_3	O	D_6	D_5	D_4	D_3
S	A_1	A_1	A_1	A_1	A_1
P	T_1	$A_2 + E_1$	$A_2 + E_1$	A_2+E	$A_2 + E$
D	$E + T_2$	$A_1 + E_1 + E_2$	$A_1 + E_1 + E_2$	$A_1 + B_1 + B_2 + E$	$A_1 + 2E$
F	$A_2 + T_1 + T_2$	$A_2 + B_1 + B_2 + 2E$	$A_1 + 2A_2 + 2E$		
G	$A_1 + E + T_1 + T_2$	$2A_1 + A_2 + B_1 + B_2 + 2E$	$2A_1 + A_2 + 3E$		
H	$E + 2T_1 + T_2$	$A_1 + 2A_2 + B_1 + B_2 + 3E$	$A_1 + 2A_2 + 4E$		

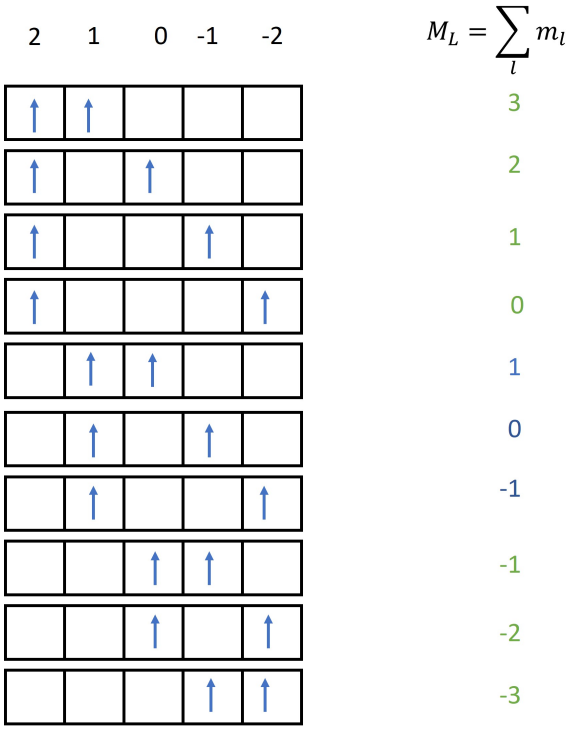

Figure 1.21: d^2 weak field microstates with M_S=1. Note the M_L=1, 0 and -1 components of the ^3F and ^3P states are mixtures of the two microstates with corresponding M_L shown in blue and green - the use of colour is simply for book-keeping purposes.

each other: this is known as *configuration interaction*. For weak fields, the lower $^3T_{1g}$ state will be made up largely of the ^3F state of the free ion while the upper $^3T_{1g}$ state will be made up mostly of the ^3P state. However, this distinction becomes less clear as the ligand-field splitting increases, and at some point the strong-field limit becomes a more logical starting point. As a result of the configuration interaction, the energies of the $^3T_{1g}$ states are not linear functions of Δ_o, and the order of the $^3T_{1g}(P)$ and A_{2g} states may swap depending on the details of the system.

The value of Δ_o is given by the difference $\nu_2 - \nu_1$ shown in Figure 1.22, but this is not always useful because the ${}^3A_{2g}$ and ${}^3T_{1g}(P)$ states can swap, so it is not necessarily obvious whether the ${}^3T_{1g}(F) \rightarrow {}^3\ A_{2g}$ transition is the second or third band in the spectrum.

Finally, we can assign the first two peaks in the spectrum of $[V(H_2O)_6]^{3+}$ to the ${}^3T_{1g}(F) \rightarrow {}^3\ T_{2g}$ and ${}^3T_{1g}(F) \rightarrow {}^3\ T_{1g}(P)$ transitions. Note that in Figure 1.23 the ${}^3A_{2g}$ state lies above ${}^3T_{1g}(P)$, and the third transition, ${}^3T_{1g}(F) \rightarrow {}^3\ A_{2g}$, in fact lies beyond the range of the spectrometer.

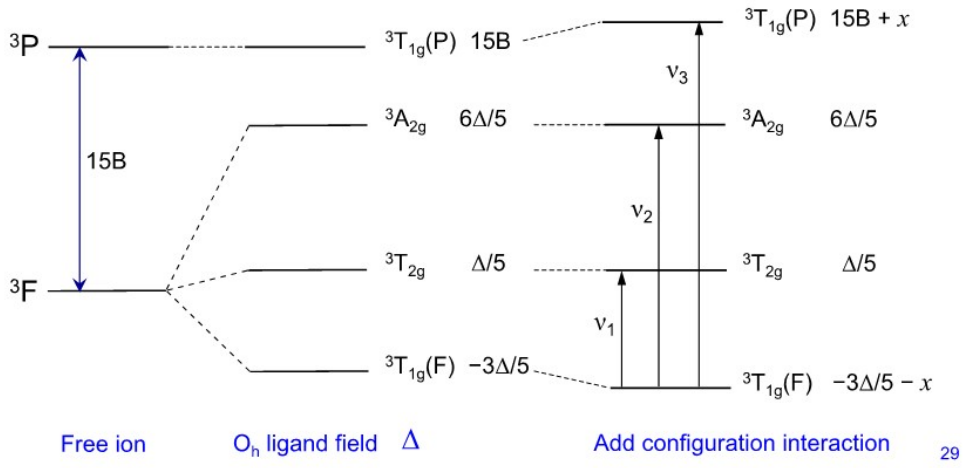

Figure 1.22: Splitting of the d^2 weak field states in an octahedral field

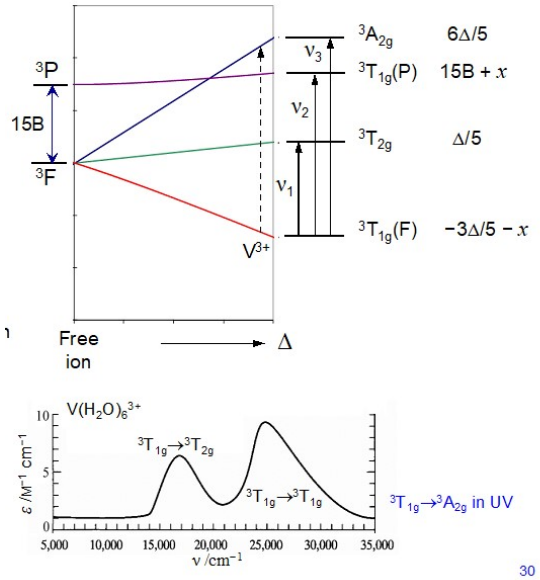

Figure 1.23: Electronic spectrum of $[V(H_2O)_6]^{3+}$

1.7.2 Spectra of d^3 ions: Strong and weak-field limits

We can develop the spectrum of the d^3 ions in exactly the same way, starting from the weak and strong-field limits. If we restrict our attention to the states of highest multiplicity ($S = \frac{3}{2}$), we can make use of the hole formalism to see that there should be many similarities between d^3 and d^2. The symmetries of the states at the strong-field limit are the same, but their energies are inverted: ${}^4A_{2g} < \{{}^4T_{1g}, {}^4T_{2g}\} < {}^4T_{1g}$. At the weak-field limit, Hund's 1st rule dictates that ${}^4F$ lies below ${}^4P$, as before. Because the ${}^4T_{1g}$ level derived from the upper ${}^4P$ level is pushed upwards by configuration, the ordering of levels is unambiguous (unlike the d^2 case where the order of ${}^3T_{1g}$ and ${}^3A_{2g}$ depends on the balance between Δ_o and B). We can again capture the essential features of both d^2 and d^3 configurations in an Orgel diagram (Figure 1.26).

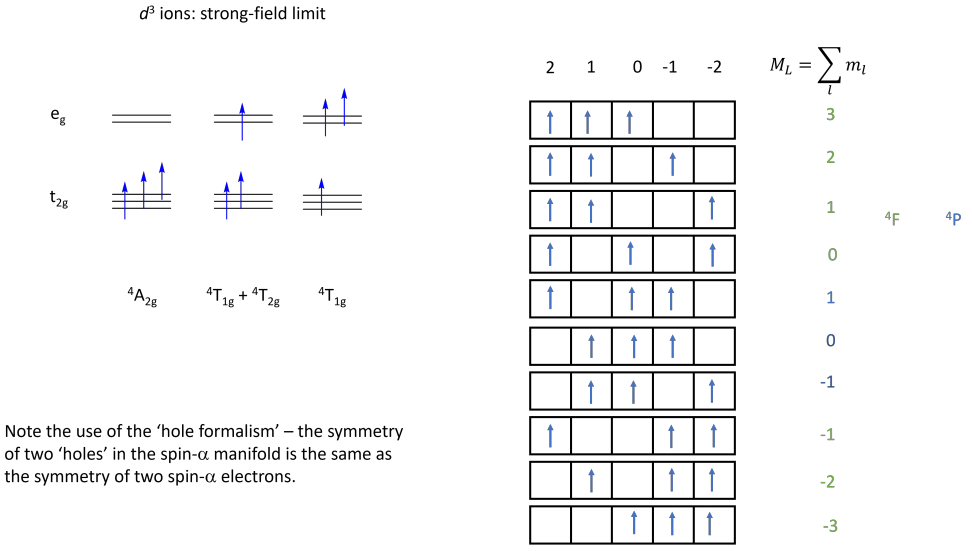

Figure 1.24: Strong and weak-field states for a d^3 ions

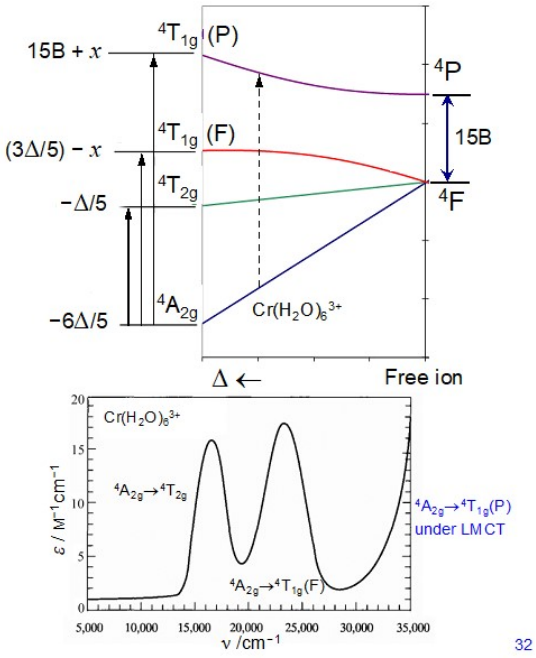

Figure 1.25: Splitting of the weak-field states of a d^3 ion in an octahedral field and spectrum of $[Cr(H_2O)_6]^{3+}$

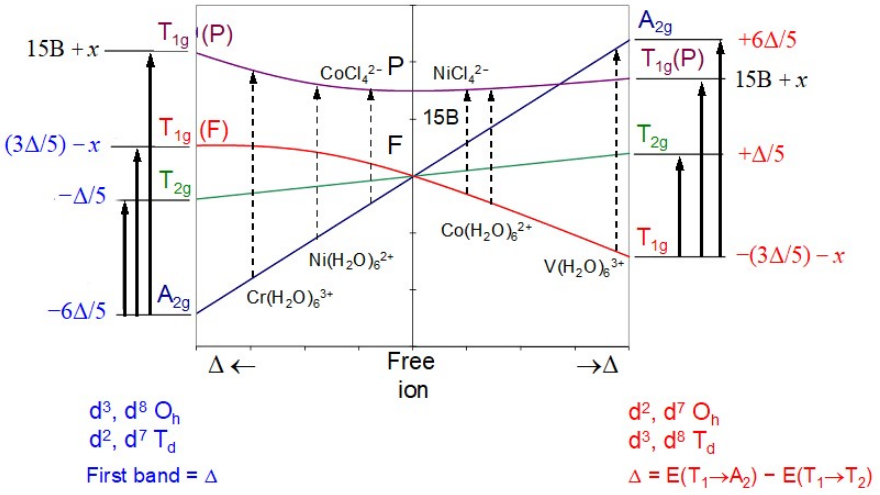

Figure 1.26: Orgel diagrams for d^2 and d^3 ions in an octahedral field.

Vertical periodic trends: Cr^{3+} *vs* Mo^{3+} The spectrum of $[Mo(H_2O)_6]^{3+}$ has the same number of bands and the same symmetries of states as $[Cr(H_2O)_6]^{3+}$, as it must because it shares the same d^3 configuration. However, if we compare the two spectra we note that the bands in $[Mo(H_2O)_6]^{3+}$:

1. appear at higher frequency
2. are more intense
3. are broader
4. are closer together, almost to the point that they merge into one.

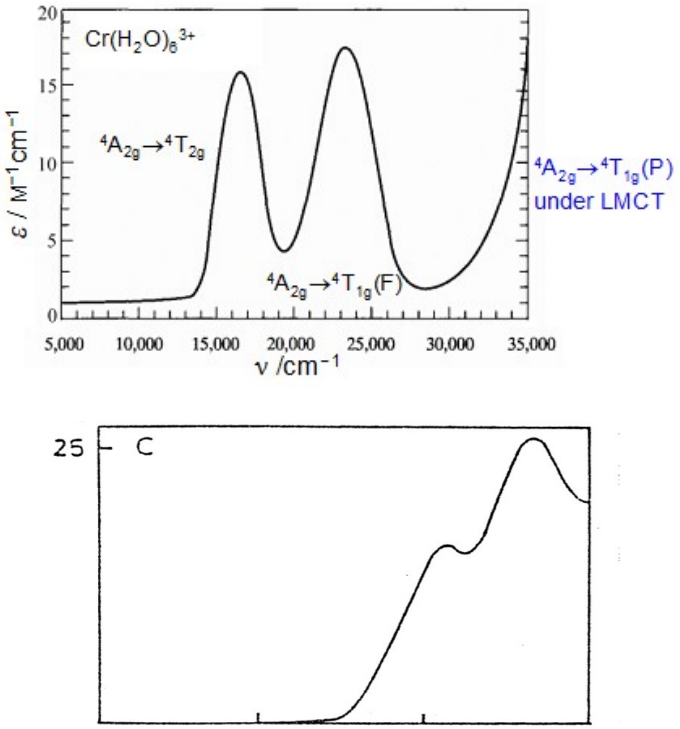

Figure 1.27: Electronic spectra of $[Cr(H_2O)_6]^{3+}$ (top) and $[Mo(H_2O)_6]^{3+}$ (bottom).

All of the above can be explained by the more diffuse nature of the $4d$ orbitals compared to $3d$. This means that the overlap with ligands is greater, which, in turn, means that the ligand-field splitting, Δ_o, is larger for Mo^{3+} (hence higher frequencies). The vibronic coupling is also stronger (hence broader, more intense bands).

The final observation, that the two lowest-frequency bands get closer together, requires more thought. The two excited states, ${}^4T_{1g}$ and ${}^4T_{2g}$, are derived from the same configuration ($t_{2g}^1 e_g^1$), and differ only in the nature of the electron-electron repulsions (Figure 1.20). In the (hypothetical) limit that the electron-electron repulsions were negligible, the two states would $\therefore$ be degenerate and the two bands would merge into one. The $4d$ orbitals of Mo have a radial node, which serves to spread the

electron density out, and hence reduce the electron-electron repulsion. So we see that the position of the bands is sensitive not just to Δ_o, but also B.

1.7.3 Spectra of d^8 ions: mirror image of d^2

We can extend the analysis to d^7 and d^8 in the same way as we did for d^6 and d^9 by noting that a full sub-shell of five spin-α electrons is totally symmetric. The splitting of levels in the d^8 system is therefore analogous to d^3 while d^7 is analogous to d^2. $[Cr(H_2O)_6]^{3+}$ and $[Ni(H_2O)_6]^{2+}$ are both identified in the Orgel diagram in Figure 1.26. $[Cr(H_2O)_6]^{3+}$ has the larger value of Δ_o because it has a +3 charge and also has more diffuse $3d$ orbitals.

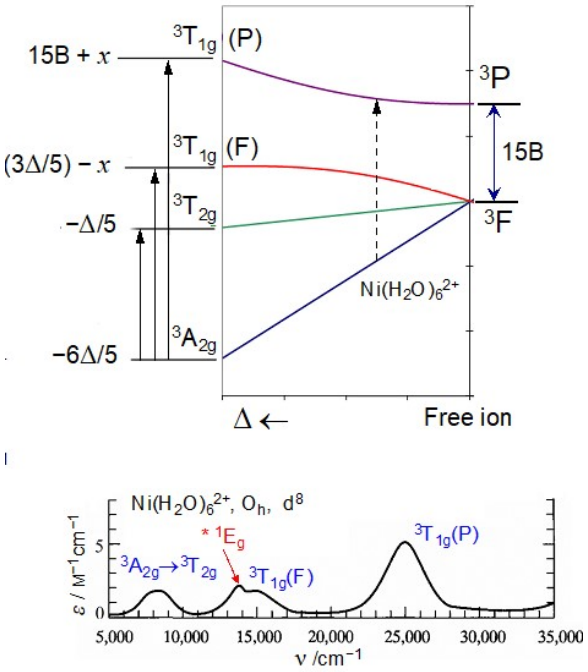

Figure 1.28: Electronic spectrum of $[Ni(H_2O))_6]^{2+}$.

An interesting feature of the spectrum of $[Ni(H_2O)_6]^{2+}$ is the presence of a spin-forbidden band ($^3A_{2g} \rightarrow ^1 E_g$) at around 14000 cm^{-1}, appearing as a shoulder to low frequency of the $^3A_{2g} \rightarrow ^3 T_{1g}(F)$ band. The spin-forbidden band gains intense through spin-orbit induced mixing of the singlet and triplet states which is particularly strong because the two states happen to be very close in energy. This mechanism is known as 'intensity stealing'.

1.7.4 Spectra of tetrahedral d^7 ions

By applying the hole formalism, we can also identify an analogy between the states of a (high-spin) d^7 ion in a tetrahedral field and those of the d^3 and d^8 ions in an octahedral field. This is also shown in the Orgel diagram in Figure 1.26: note that the value of Δ is now much lower than for typical octahedra - $\Delta_t \approx \frac{4}{9}\Delta_o$.

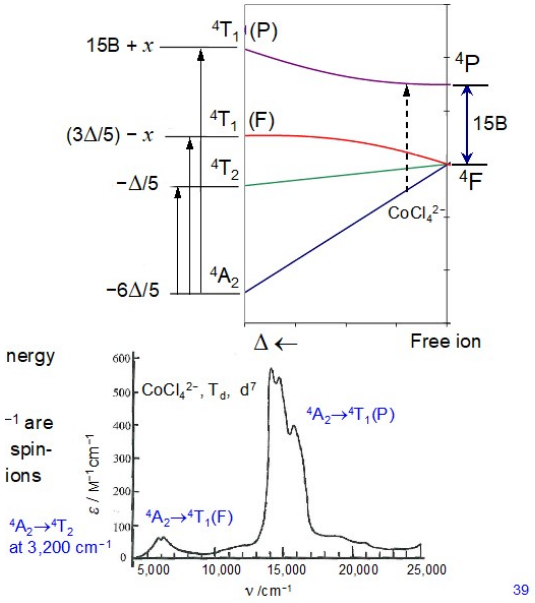

Figure 1.29: Electronic spectrum of $[CoCl_4]^{2-}$.

1.8 Quantitative models: Tanabe-Sugano Diagrams

The Orgel diagrams used in the previous section are useful from a qualitative perspective: they show the splitting of states in ligand fields of various strengths, and they emphasise the relationship between different configurations. However, the only variable in an Orgel diagram in Δ: B, in contrast, is fixed (usually at the free-ion value), and to explore the effects of changing B, we would need a series of different Orgel plots. Tanabe and Sugano sokved this problem by dividing both axes are divided through by B, the Racah parameter. The x axis is now defined by the ratio of $\frac{\Delta}{B}$ (or $\frac{Dq}{B}$ where $\Delta_o = 10Dq$). The vertical axis is then $\frac{E}{B}$, where E is the energy of transition. E, Δ and B all have units of cm^{-1}, so the ratios are dimensionless. In Tanabe-Sugano diagrams, the zero of energy is always the ground state, which may change as a function of $\frac{Dq}{B}$, leading to discontinuities in the graph. The key point is that the Tanabe-Sugano diagram is valid for any combination of Δ and B, and it can be used to determine both from the experimental data.

From a knowledge of two or more transition energies, we can use the Tanabe-Sugano diagrams to extract values of Δ_o and B. Recall that in some cases one of the transitions corresponds directly to Δ_o but in others Δ_o corresponds to the difference of two bands, one of which may not be observable.

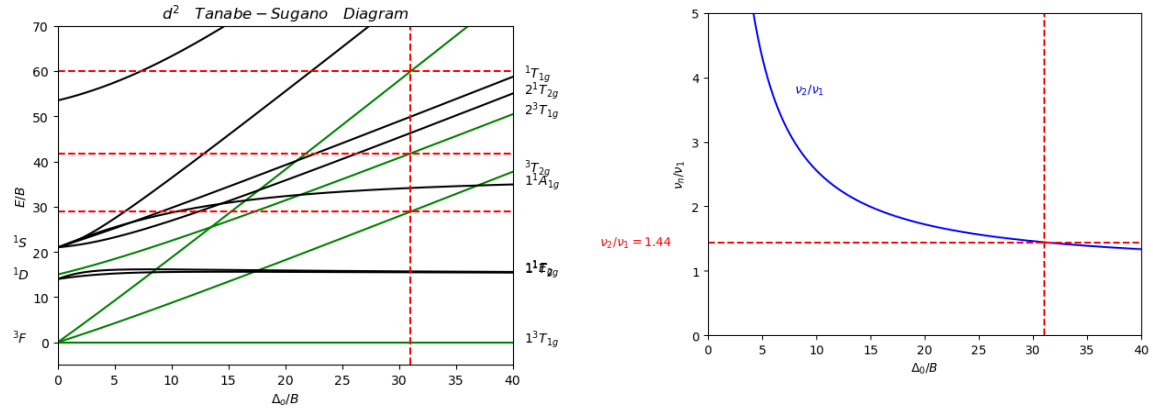

Figure 1.30: Tanabe-Sugano diagram for d^2. Green lines are the triplet states. Red dashed lines show the best match to the experimental data for $[V(H_2O)_6]^{3+}$. The plot on the right shows the ratio of ν_2/ν_1 as a function of Δ_o/B - the point at which the curve intersects the horizontal line $\nu_2/\nu_1 = 1.44$ identifies the best-fit value for Δ_o/B (it is ≈ 31).

Example: $[V(H_2O)_6]^{3+}$ has two bands in the visible region, neither of which corresponds directly to Δ_o:

$\nu_1 = 17800$ cm^{-1} ($^3T_{1g}(F) \rightarrow^3 T_{2g}$) and $\nu_2 = 25700$ cm^{-1} ($^3T_{1g}(F) \rightarrow^3 T_{1g}(P)$)

$$\frac{\nu_2}{\nu_1} = 1.44$$

We could then plot the ratio $\frac{\nu_2}{\nu_1}$ as a function of $\frac{\Delta_o}{B}$ and identify the point where it equals 1.44. This is shown on the right of Figure 1.30. In practice (or in an exam!), we would simply read off a few values of ν_1 and ν_2 and interpolate to identify (approximately) the value that gives the best match to experiment: it is $\frac{\Delta_o}{B} \approx 31$. Note there is some guesswork involved here - anywhere around 30-35 would do!

The vertical line at $\frac{\Delta_o}{B} = 31$ intersects $^3T_{1g} \rightarrow^3 T_{2g}$ at $\frac{E}{B} = 29$ and $^3T_{1g}(F) \rightarrow^3 T_{1g}(P)$ at $\frac{E}{B} = 42$

From the first point: $\frac{17800}{B} = 29$, $B = \frac{17800}{29} = 614$ cm^{-1} $\therefore \frac{\Delta_o}{614} = 31$, $\Delta_o = 31 \times 614 = 19034$ cm^{-1}.

From the second point: $\frac{25700}{B} = 42$, $B = \frac{25700}{42} = 612$ cm^{-1} $\therefore \frac{\Delta_o}{612} = 31$, $\Delta_o = 31 \times 612 = 18972$ cm^{-1}.

Averaging: $B = 613$ cm^{-1}, $\Delta_o = 19000$ cm^{-1}.

In Section 1.7.1 we noted that the third band in the spectrum of $[V(H_2O)_6]^{3+}$, $^3T_{1g}(F) \rightarrow^3 A_{2g}$, was outside the range of the spectrometer: we can now predict that it should appear at $60B = 36400$ cm^{-1}.

Tanabe-Sugano diagrams for d^5, d^6 and d^8 are shown in Figure 1.31. Note the discontinuities for d^5 and d^6 at $\frac{Dq}{B} \approx 2.8$ and 1.9, respectively, that mark the spin-crossover between a high-spin ground state (at low $\frac{Dq}{B}$) and a low-spin ground state. The dashed lines in the diagram for the d^8 system mark the approximate value of $\frac{Dq}{B}$ for $[Ni(H_2O)_6]^{2+}$, the spectrum of which is shown in Figure 1.28 - note the coincidental near-degeneracy of the 1^1E_g and $1^3T_{1g}(P)$ states at this point.

1.9 Spectrochemical and nephelauxetic series

The spectrochemical series compares ligand effects on Δ_o (see Bonding in Molecules, year 2)

The nephelauxetic (cloud expansion) series compares ligand effects on the Racah parameter, B

B is a measure of electron-electron repulsion, so any factor that increases the average separation of the electrons will reduce B. The nephelauxetic ratio: $\beta = \frac{B_{complex}}{B_{free\ ion}}$

Table 1.7: Values of the Racah parameter, B, in cm^{-1}. Values of β are given in parenthesis.

	$\mathbf{M^{2+}}$	$\mathbf{[M(H_2O)_6]^{2+}}$	$\mathbf{[M(NH_3)_6]^{2+}}$
V^{2+}	860	660 (0.77)	
Mn^{2+}	960	770 (0.80)	
Ni^{2+}	1080	870 (0.81)	810 (0.75)

nephelauxetic series: $F^- < H_2O < NH_3 <$ en $<$ oxalate$^{2-} < Cl^- \sim CN^- < Br^- < I^-$
spectrochemical series: $I^- < Br^- < Cl^- < F^- < H_2O <$ oxalate$^{2-} < NH_3 <$ en $< CN^-$

The nephelauxetic effect is broadly similar for π-donor and π-acceptor ligands, in marked contrast to the spectrochemical series.

1.10 Ligand-to-metal charge transfer (LMCT) spectra

1.10.1 Intensities

Ligand-to-metal charge-transfer (LMCT) transitions involve the transfer of an electron from a ligand-based orbital to one on the metal. From a group theoretical point of view these transitions are often allowed ($e \rightarrow t_2$ in tetrahedral $[MnO_4]^-$, for example), but no more allowed in a strict group-theoretical than the $d \rightarrow d$ transition in $[CoCl_4]^{2-}$. However, charge-transfer transitions are typically orders of magnitude more intense than $d \rightarrow d$ transitions, irrespective of the symmetry.[4] Once again, we need to separate out the question of whether $Q = 0$ or not (which we answer with group theory) from the question of what factors make Q large in the event that group theory confirms that it is not zero.
Consider the lowest LMCT band in tetrahedral $TiCl_4$: it is a $t_1 \rightarrow e$ transition, so allowed from a group theoretical perspective. So we then move on to the second question which is why Q might be

[4]Examiners will often use the expression 'intense transition' to alert you to the fact that it is an LMCT transition, not a $d \rightarrow d$ transition

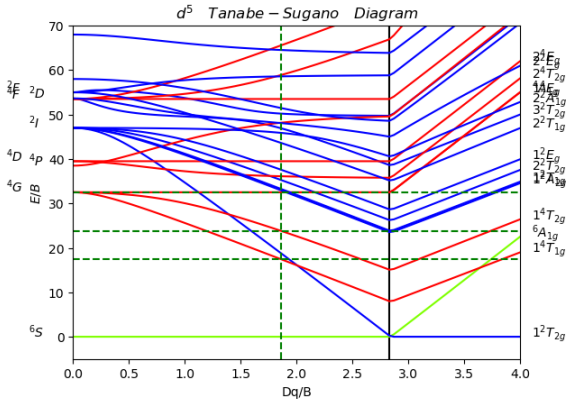

(a) Tanabe-Sugano diagram for a d^5 ion.

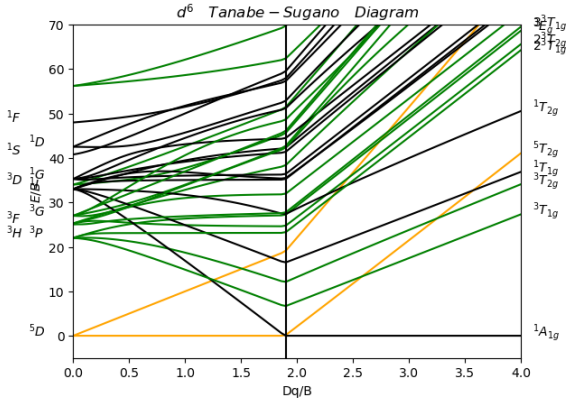

(b) Tanabe-Sugano diagram for a d^6 ion.

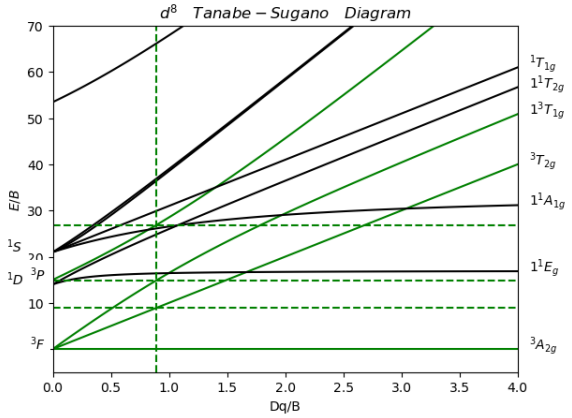

(c) Tanabe-Sugano diagram for a d^8 ion.

Figure 1.31: Tanabe-Sugano diagrams for d^5, d^6, d^8 cases

large for LMCT and smaller (albeit not quite zero) for $d \rightarrow d$ transitions. Recall the expression for the transition dipole moment:

$$Q = \int \psi_f \hat{\mu} \psi_i d\tau = -e \int \psi_f r \psi_i d\tau \tag{1.10.1}$$

The 'r' in this expression reflects the distance that the electron travels during the transition and Mulliken has shown that the intensity of an LMCT transition is proportional to r, the metal-ligand bond length. So the extremely high intensity of allowed LMCT transitions stems from the simple fact that the electron moves a long way in the course of the transition.

1.10.2 Trends in LMCT energies

LMCT transitions can, to a good approximation, be regarded as internal redox processes, where the ligand(s) are oxidised and the metal is reduced. So trends in LMCT tend to mirror trends in electron affinities (the negative of the ionisation energy): any factor that makes the reduction of the metal easier will lower LMCT, as will anything that makes oxidation of the ligand easier. Things to look out for include:

1. trends in Z_{eff} across a period (it increases)
2. trends in Z_{eff} down a group (it decreases)
3. oxidation states (higher oxidation will lower LMCT)
4. filling of sub-shells (discontinuities when the t_{2g} shell is filled, for example).
5. effects of half-filled shells (particularly important in 1st-row TMs). If the ground state has a half-filled shell, the LMCT will be raised in energy whereas if the excited state has a half-filled shell, it will be lower.

Tetrahedral complexes There are a wide range of tetrahedral transition metal complexes containing halides and chalcogenides - these provide a rich source of data for 'orbital mapping' (Figure 1.32) The basic features of the frontier orbital domain are the same in all cases: the lowest frequency intense transition is $t_1 \rightarrow e$ or, if the e level is filled, $t_1 \rightarrow t_2$.

Points to note

1. Descending the halide group (Cl $\rightarrow$ Br), the valence np orbitals increase in energy, with the result that LMCT energies go down by about 5000-10000 cm^{-1}.
2. Increasing oxidation of Fe stabilises the $3d$ orbitals, reducing LMCT energy. Change is $\sim$ 18000 cm^{-1} per unit charge.
3. LMCT in the first-row M^{II} chlorides does down across the series due to increasing Z_{eff}. Discontinuity at Zn because the d-shell is full, so LMCT goes to a higher orbital (Zn $4s$).
4. Vertical trends in the oxides: LMCT increases down the group, Cr $\rightarrow$Mo $\rightarrow$W or Mn $\rightarrow$Tc $\rightarrow$Re. nd orbitals become relatively higher in energy as we descend a group. Note $4d$ and $5d$ are quite similar to each other (gap $\sim$7000 cm^{-1}) while $3d$ is quite different (gap $\sim$17000 cm^{-1}). This is the effect of the lanthanide contraction, stabilising $5d$.

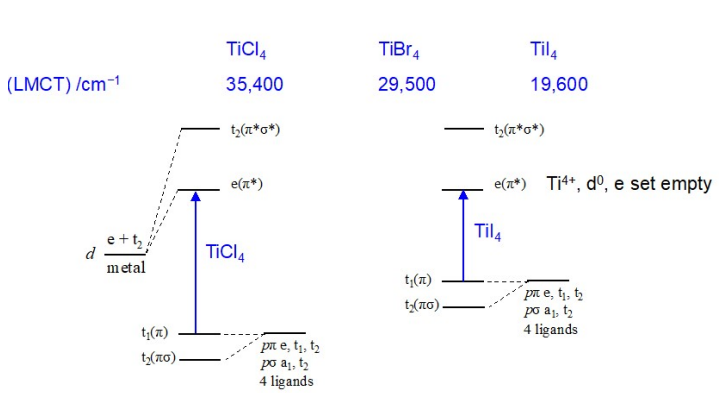

(a) Charge-transfer spectra of Ti halides.

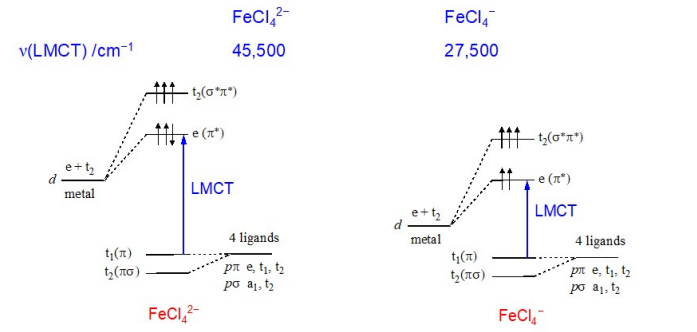

(b) Charge-transfer spectra of Fe chlorides.

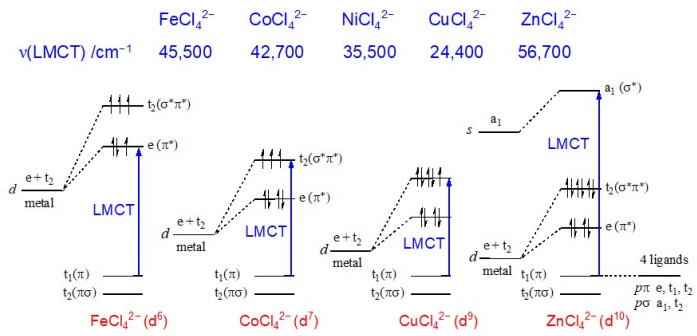

(c) Charge-transfer spectra of first-row chlorides.

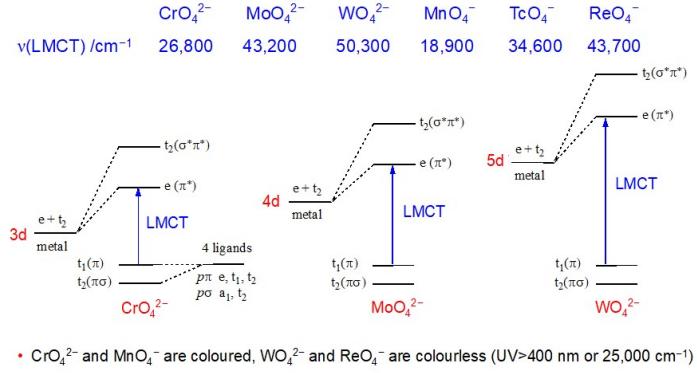

(d) Charge-transfer spectra of metal oxides, $[MO_4]^{z-}$.

Figure 1.32: LMCT in tetrahedral complexes.

LMCT in Octahedral complexes Similar trends can be identified in the octahedral complexes, Table 1.8:

Points to note

1. Descending the halide group (Cl → Br), the valence np orbitals increase in energy, with the result that LMCT energies go down by about 5000-10000 cm^{-1}.
2. Across the $4d$ transition metals (Zr → Pd) Z_{eff} increases, lowering the $4d$ orbitals and reducing the LMCT energy. Overall stabilisation is worth ∼ 20000 cm^{-1} from Zr (t_{2g}^0) to Ru (t_{2g}^5) There is a big jump at Pd, where the $2t_{2g}$ level is filled, so the transition is ν_2 rather than ν_1.
3. The trend Zr → Mo → Tc is very non-linear: $[MoCl_6]^{2-}$ looks high and/or $[TcCl_6]^{2-}$ looks low. $[TcCl_6]^{2-}$ has a d^3 configuration, so a half-filled t_{2g}^3 shell. LMCT therefore places an electron of opposite spin in the t_{2g} shell, which is not stabilised by exchange (or is destabilised by strong e-e repulsions, whichever way you choose to look at it). The excited state is unstable, so LMCT is higher in energy than it would be in the absence of exchange effects. Conversely, $[MoCl_6]^{2-}$ is d^2, so LMCT completes the half-filled t_{2g}^3 shell, stabilising the excited state.
4. A similar trend is apparent across the $5d$ series (W → Pt), but transition energies are ∼ 10000 cm^{-1} higher than their $4d$ counterparts. $5d$ orbitals are higher in energy than $4d$ - the normal trend down a group, enhanced here by relativistic destabilisation of $5d$.
5. The same trend is observed for Fe → Ru → Os, but Fe looks high (we would expect Ru and Os to be relatively similar due to the lanthanide contraction, and quite different to Fe). Fe is high-spin d^5, the others are low-spin. LMCT into a half-filled shell carries an energetic penalty because it creates a d^6 configuration, where the 6th electron is not stabilised by exchange.
6. Increasing oxidation state of W lowers the $5d$ orbitals, reducing LMCT by ∼7000 cm^{-1} per unit charge. Note this is much less than for Fe (∼7000 cm^{-1} per unit charge) - this reflects the well-known tendency of heavier transition metals to adopt higher oxidation states ("more penetrating orbitals are less sensitive to charge")
7. In the comparison of $[FeCl_4]^-$ and $[FeCl_6]^{3-}$ (both Fe^{III}, both Cl^-), the LMCT band is distinctly higher in the tetrahedral complex (27500 cm^{-1} compared to 24900 cm^{-1}). The difference lies in the right hand-side of the MO diagrams: the ligand-based levels span a range of energies due to overlap between the p orbitals (lone-pair-lone-pair repulsions in a different guise), and the uppermost levels from which the lowest LMCT transitions emanate are antibonding. Antibonding overlap is greater in the octahedron simply because the Cl^- ions are forced closer together, so the octahedral t_{1u} orbital is higher in energy than the tetrahedral t_1, so LMCT occurs at lower frequency. Same for Fe^{II}.

Table 1.8: LMCT transition energies in metal hexa-halides

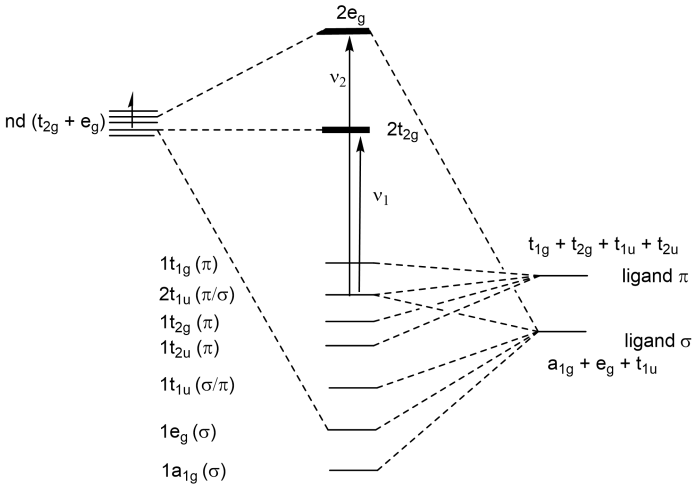

Cl/Br comparison	Nb^{V} d^0	Ta^{V} d^0		Ru^{IV} d^4	Rh^{III} d^6	
	$[NbCl_6]^-$	$[TaCl_6]^-$		$[RuCl_6]^{2-}$	$[RhCl_6]^{3-}$	
	31800	38000		19400	41000	
	$[NbBr_6]^-$	$[TaBr_6]^-$		$[RuBr_6]^{2-}$	$[RhBr_6]^{3-}$	
	23800	>24000		15800	28600	
Pt^{IV} complexes d^6	$[PtF_6]^{4-}$	$[PtCl_6]^{4-}$	$[PtBr_6]^{4-}$	$[PtI_6]^{4-}$		
	>45000	37000	30600	20300		
M^{IV} chlorides d^n	$[ZrCl_6]^{2-}$	$[MoCl_6]^{2-}$	$[TcCl_6]^{2-}$	$[RuCl_6]^{2-}$	$[RhCl_6]^{2-}$	$[PdCl_6]^{2-}$
	41700	24500	22000	19400	12000	29400
		$[WCl_6]^{2-}$	$[ReCl_6]^{2-}$	$[OsCl_6]^{2-}$	$[IrCl_6]^{2-}$	$[PtCl_6]^{2-}$
		36500	32000	26000	19700	37000
group 8 M^{III} chlorides d^5	$[FeCl_6]^{3-}$	$[RuCl_6]^{3-}$	$[OsCl_6]^{3-}$			
	24900	28600	35400			
variable oxidation states	$[WCl_6]^{3-}$	$[WCl_6]^{2-}$	$[WCl_6]^-$			
	45000	36500	29400			
coordination number	$[FeCl_6]^{4-}$	$[FeCl_4]^{2-}$	$[FeCl_6]^{3-}$	$[FeCl_4]^{1-}$		
	42800	45500	24900	27500		

1.10.3 Vibrational fine structure in LMCT transitions

We saw in section 1.6.2 that vibronic coupling makes $d \rightarrow d$ transitions that would otherwise be forbidden allowed. The LMCT transitions in *e.g.* $[MnO_4]^-$ are perfectly allowed, so vibronic coupling isn't a requirement for significant intensity. Nevertheless it is still present, and we can see coupling of vibrational and electronic modes. The vibrational progression in the ν_1 transition in Figure 1.33 is due to coupling to the symmetric stretching mode (A_1 symmetry) of the excited state. The separation between the peaks is approximately 770 cm^{-1} compared to a value of 834 cm^{-1} for the ground state (measured by Raman spectroscopy). The LMCT transition populates the orbital of e symmetry which has Mn-O π^* character, so the Mn-O bond gets weaker in the excited state and the symmetric stretch is at lower frequency.

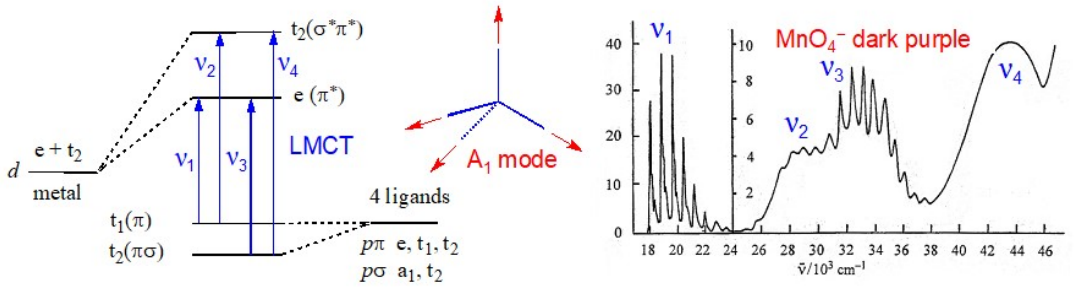

Figure 1.33: Charge-transfer spectrum of $[MnO_4]^-$ showing the vibrational progression due to the totally-symmetric mode.

1.11 Metal-to-ligand charge transfer (MLCT) spectra

This class is rather less common than the LMCT, but intense MLCT can sometimes be observed with strong π-acceptor ligands, which have low-lying vacant π^* orbitals that can act as acceptors. Most of these complexes are 18-electron d^6 species, so there is less variety than in the LMCTs. The trends in transition energies are the reverse of the LMCTs: the process can be viewed as an oxidation of the metal with concomitant reduction of the ligand, so any factor that favours oxidation of the metal will lower the energy of the MLCT and *vice versa*.

Table 1.9: MLCT transition energies (in cm^{-1}) in metal hexa-carbonyls

$[Nb(CO)_6]^-$	$Mo(CO)_6$	$[Tc(CO)_6]^+$
not measured	34900	not measured
$[V(CO)_6]^-$	$Cr(CO)_6$	$[Mn(CO)_6]^+$
28400	35700	44500
$[Ta(CO)_6]^-$	$W(CO)_6$	$[Re(CO)_6]^+$
26200	34600	44500

Points to note:

1. There is much less difference between $3d$, $4d$ and $5d$ than there was in the LMCT. All complexes are low-spin d^6, so we don't see the fluctuations due to oxidation state or spin state.
2. Increasing positive charge stabilises the nd orbitals by $\sim$8000 cm^{-1} per unit charge, as we saw for $[WCl_6]^{z-}$.

2 Magnetic Properties of Metal Complexes

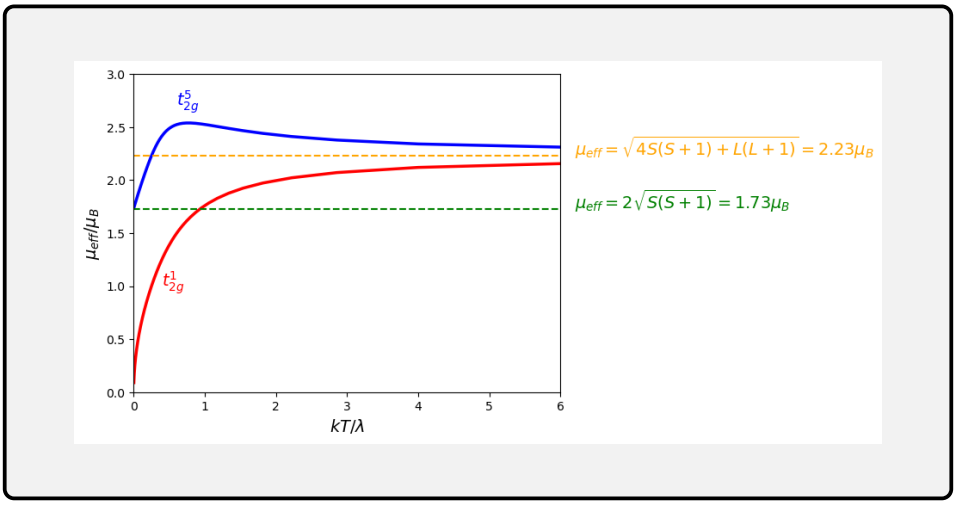

Bibliography:
Coverage of magnetism in general inorganic texts does not often go beyond a superficial coverage of the spin-only formula. For more specialised reading, see:

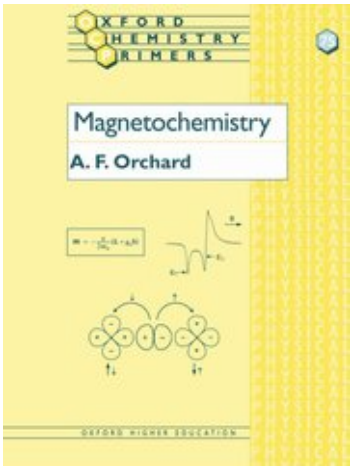

(a) Orchard, *Magnetochemistry.*

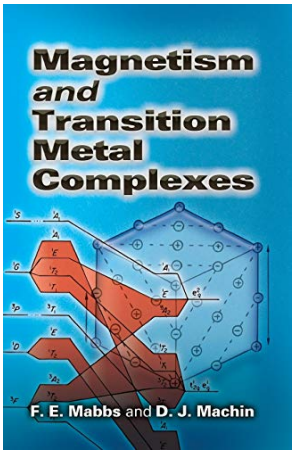

(b) Mabbs and Machin, *Magnetism and Transition Metal Complexes.*

You have encountered the magnetic properties of inorganic complexes already, in two different contexts. The 'spin-only' formula that explains the magnetic properties of most first-row transition metals:

$$\mu_{SO} = 2\sqrt{S\left(S+1\right)}\mu_B \tag{2.1}$$

and the Landé formula, which works well for most lanthanide complexes:

$$\mu_{eff} = g_J\sqrt{J\left(J+1\right)}\mu_B \tag{2.2}$$

$$g_J = 1 + \frac{J\left(J+1\right) - L\left(L+1\right) + S\left(S+1\right)}{2J\left(J+1\right)}$$

are familiar from years 1 and 2. The purpose of this course is to take a wider look at the magnetic properties of metal complexes (transition metals and lanthanides) to understand where these formulae come from and, most importantly, why they often don't work. The subject is intrinsically quantum mechanical - all the key formulae are derived from perturbation theory. However, we can identify types of behaviour that are characteristic of particular ground-state symmetries without understanding all of the details!

In Table 2.1 the magnetic properties of a range of transition metal complexes are collected: some correspond almost exactly to the spin-only formula (μ_{SO}) but rather more that do not. Even when the agreement is good, this may be coincidental (this is the case for K_2FeO_4, as we will see later). We also see that μ_{eff} is usually independent of temperature, but there are some cases where it varies widely.

The starting point for the interpretation of magnetic properties of transition metal complexes is always the spin-only formula, so it is worth keeping in mind the values of μ_{SO} for 1 to 5 unpaired electrons that emerge from Equation 2.1 (in units of μ_B, the Bohr magneton): d^1 1.73; d^2 2.83; d^3 3.87; d^4 4.90; d^5 5.92. Examiners will often give you these values at the start of a question as a guide.

Table 2.1: **Magnetic properties of selected transition metal complexes.**

compound	μ_{eff}/μ_B	Temp dep?	Configuration	State	unpaired e^-	μ_{so}/μ_B
$Cr(\eta^6-C_6H_6)_2$	0.0	No	Cr^0, O_h, d^6, $e_g^4 a_{1g}^2$	$^1A_{1g}$	0	0.
$[Mn(H_2O)_6]^{2+}$	5.90	No	Mn^{2+}, O_h, d^5, $t_{2g}^3 e_g^2$	$^6A_{1g}$	5	5.92
$[Mn(CN)_6]^{3-}$	2.18	Yes	Mn^{2+}, O_h, d^5, ${t_{2g}}^5$	$^2T_{2g}$	1	1.73
$[FeO_4]^{2-}$	2.83	No	Fe^{6+}, T_d, d^2, e^2	$^3A_2$	2	2.83
$[ReF_6]^{2-}$	3.50	No	Re^{4+}, O_h, d^3, t_{2g}^3	$^4A_{2g}$	3	3.87
${CoCl_4}^{2-}$	4.47	No	Co^{2+}, T_d, d^7, $e^4 t_2^3$	$^4A_2$	3	3.87

2.1 Magnetism: some definitions and techniques

2.1.1 Classical magnetism

A magnetic moment m (SI unit Bohr magneton, μ_B) is generated by a current I flowing through a loop of area A. This moment will tend to align parallel to a magnetic field H ($\theta = 0$). The unit of magnetic field is Tesla (T). For context, the magnetic field at the surface of the earth is $\sim 5 \times 10^{-5}$T while a typical fridge magnet has a field of ~ 0.02T.

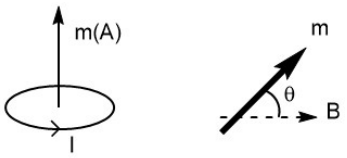

Figure 2.2: Definition of a magnetic moment.

2.1.2 Susceptibilities

If a body is placed in a homogeneous magnetic field, the field within the body, B (the magnetic induction), will be different from the field in free space, H.

$$B = H + M$$

where M is the magnetisation, the magnetic moment induced per unit volume. The central quantity that is used in magnetic studies is the magnetic susceptibility, χ, which is defined as:

$$\chi = \frac{M}{H}$$

It is generally more convenient to measure mass than volume, so we can convert the volume susceptibility, χ, to the molar susceptibility, χ_{mol}, which has units of $m^3 mol^{-1}$:

$$\chi_{mol} = \chi \times \frac{M_r}{1000\rho}$$

Any measurement of magnetic susceptibility depends on measuring the ratio of the magnetic induction to the free field, $\frac{B}{H}$. This can be done using a Gouy balance or, in more modern applications, a superconducting quantum interference device (SQUID) magnetometer.

(a) A Gouy balance (b) A SQUID magnetometer

Figure 2.3: Methods of measuring magnetic moments

We can connect these macroscopic ideas to molecular systems by noting that the magnetization is related to change of energy of the body in a magnetic field. If the energy of the system is reduced (stabilised) by the magnetic field, M and χ are positive and it will move to the region of highest field (we say it is *paramagnetic*). Conversely, if the energy of the system is raised by the magnetic field, χ is negative and it will be repelled from the field (we say it is *diamagnetic*). Calculations of χ and μ_{eff} are based on calculating the change in energy that the molecule undergoes when placed in a magnetic field.

- $\chi > 0$ paramagnetic
- $\chi < 0$ diamagnetic

2.1.3 Diamagnetic Susceptibilities

The total susceptibility, χ, is the sum of negative diamagnetic and positive paramagnetic contributions:

$$\chi_{tot} = \chi^D + \chi^P$$

χ^D is always present in molecules but, where there is also a source of paramagnetism, χ^P is usually large and swamps the smaller negative χ^D. However, if we want really accurate values of χ^P, we need to subtract off χ^D from the χ_{tot} that we measure.

χ_D is essentially additive, and depends to a very good approximation only on the number and type of atoms present. Pascal has published tables of constants ('Pascal's constants') that allow us to calculate χ^D for any given composition (Table 2.2). Note that Pascal's constants scale approximately with the mass of the atom. This suggests an even more extreme approximation, $\chi^D = kM \times$

10^{-6}cm^{3}mol^{-1} where k is a constant (typically 0.4-0.5) and M is the molecular mass. In this course we are concerned with understanding the magnetic behaviour at a qualitative level, so we will not concern ourselves further with these small diamagnetic corrections,

Table 2.2: **Pascal's constants for some atoms.**

atom	χ^D **(10^{-6}cm^{3}mol^{-1})**
H	-2.93
B	-7.00
C	-6.00
C (ring)	-6.24
N (open chain)	-5.57
O	-4.60
F	-6.30
Cl	-20.10
Br	-30.60
I	-44.60

2.2 Paramagnetism and the first-order Zeeman effect.

The starting point for an analysis of paramagnetism is the Zeeman effect, which can be divided into first- and second-order components. We start here with the first-order effect and then come back to second-order effects in the discussion of Temperature-Independent Paramagnetism (TIP).[5]

The Zeeman operator, equation 2.2.1 acts on both spin and orbital components of the angular momentum. The anomalous g-factor for spin means that the splitting of levels defined by different M_S is almost exactly twice as large as levels that differ by the same M_L at the same field.

$$\hat{H}_{Zeeman} = -\gamma_e(\hat{L} + g_e\hat{S})H \tag{2.2.1}$$

$$E(M_S) = \langle M_S|\hat{H}|M_S\rangle = -\gamma_e g_e H \langle M_S|\hat{S}|M_S\rangle = -\gamma_e \hbar g_e M_S H = g_e M_S \mu_B H \tag{2.2.2}$$

$$E(M_L) = \langle M_L|\hat{H}|M_L\rangle = -\gamma_e H \langle M_L|\hat{L}|M_L\rangle = -\gamma_e \hbar M_L H = M_L \mu_B H \tag{2.2.3}$$

$$g_e = 2.0023 \qquad \mu_B = -\gamma_e \hbar$$

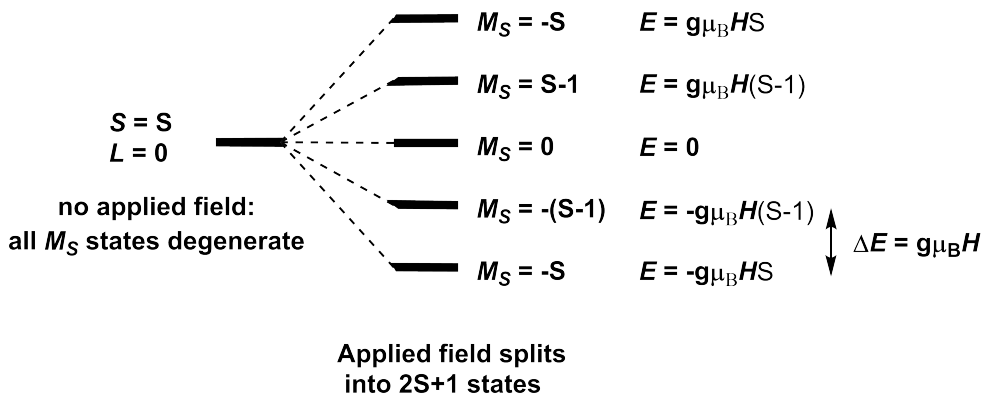

Figure 2.4: First-order Zeeman Splitting of a state with multiplicity $2S + 1$.

First-order Zeeman splitting is small - $\Delta E \sim 1$ cm^{-1} compared to $kT \sim 200$ cm^{-1} at 298 K, so Boltzmann statistics will be central to the analysis.

[5]The terms *first order* and *second order* come from the language of perturbation theory. If states are degenerate in the absence of a perturbation, then when the perturbation is turned on, their response is generally proportional to the strength of the perturbation (*1st order*). If the states are not degenerate then the response depends on the square of the strength of the perturbation, hence '*2nd order*'.

2.2.1 van-Vleck theory for an isolated ground-state with only spin angular momentum

. Let us assume that the molecule has only a single low-lying spin state, and the only source of angular momentum is spin (*i.e.* no orbital angular momentum). The best examples of this type are high-spin d^5 complexes of first row transition metal ions such as Mn^{2+} and Fe^{3+}, or f^7 lanthanide ions, Eu^{2+} and Gd^{3+}, where all excited states necessarily involve a spin-flip and lie far above the ground state as a result. The derivation of the van-Vleck equation is given in the textbooks noted in the bibliography, but the essential features are as follows:

1. The population of a given M_S level in Figure 2.4 is defined by a Boltzmann distribution:

$$P_{M_S} = \frac{exp(\frac{-E_{M_S}}{kT})}{\sum\limits_{M_S} exp\left(\frac{-E_{M_S}}{kT}\right)}$$

2. The magnetisation per mole, M, is the magnetisation per state, m_{M_S}, multiplied by the Boltzmann weighting of the state, multiplied by Avogadro's number.

$$M = N_A \sum_{M_S} m_{M_S} P_{M_S} = N_A \sum_{M_S} \frac{m_{M_S} exp\left(\frac{-E_{M_S}}{kT}\right)}{\sum\limits_{M_S} exp\left(\frac{-E_{M_S}}{kT}\right)}$$

3. The magnetisation of each state is $\frac{dE_i}{dH}$, the change in energy per unit change in field. From equation 2.2.2 and Figure 2.4, this is, to first order, $g_e M_S \mu_B$.

4. We can set the lowest energy level to $E = 0$ and then, if $E_{M_S} << kT$, we can use $exp(-x) \approx 1 - x$ (and quite a lot of further manipulation!) to simplify the above expression to:

$$M = \left[\frac{N_A \mu_0}{3kT} g_e^2 \mu_B^2 S(S+1)\right] H$$

5. The magnetic susceptibility χ is defined as

$$\chi_{mol} = \frac{M}{H} = \frac{N_A \mu_0}{3kT} g_e^2 \mu_B^2 S(S+1)$$

6. Defining the square of the spin-only magnetic moment as:

$$\mu_{SO}^2 = g_e^2 \mu_B^2 S(S+1)$$

we have:

$$\boxed{\chi_{mol} = \frac{N_A \mu_0}{3kT} \mu_{SO}^2 = \left(\frac{N_A \mu_0}{3k}\right) \mu_{SO}^2 \frac{1}{T} = \frac{C}{T}} \tag{2.2.4}$$

where C is the *Curie constant* and

$$\mu_{SO} = \sqrt{\frac{3kT\chi_{mol}}{N_A\mu_0}} = g_e\mu_B\sqrt{S(S+1)}$$

7. Finally, if we approximate $g_e \approx 2.0$, we recover:

$$\mu_{SO} = 2\mu_B\sqrt{S(S+1)}$$

A typical 'Curie law plot' of χ_{mol} *vs* T is shown in Figure 5 (blue line) - it varies as $\frac{1}{T}$. We can understand why this is by referring to the first-order Zeeman splitting in Figure 2.4. At (very) low temperatures, the difference in population between the lower levels with negative M_S and the upper ones with positive M_S will be significant, and so there is a large net stabilisation of the molecule when we turn the field on (*i.e.* a large susceptibility). At higher temperatures, the population of levels with positive and negative M_S are approximately equal, and so there is almost no net stabilisation in a magnetic field, hence low susceptibility. If the Curie law is obeyed, the inverse susceptibility plot, χ_{mol}^{-1} *vs* T (in green) should be linear and should pass through the origin.

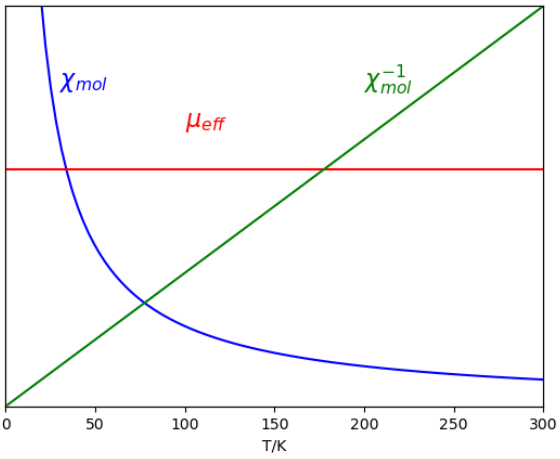

Figure 2.5: Curie-law behaviour for an isolated ground state.

It is important to emphasise that the susceptibility, χ is the fundamental property that we measure in a magnetic experiment. However, the temperature dependence of χ makes it difficult to work with - if we wanted to compare materials, which temperature would we choose to define χ at? It would be convenient to have a single number that is independent of temperature that we could use to characterise the magnetic properties of a molecule. This is where μ comes in: if the system obeys the Curie law then $\mu_{eff} = \mu_{SO} = \sqrt{\frac{3KT\chi_{mol}}{N_A\mu_0}} \propto \sqrt{\chi_{mol}T}$, which is *independent* of temperature. Of course, if the system does not obey the Curie law (and most systems don't!) then μ_{eff} becomes dependent on temperature and the analysis becomes more complex (and more interesting).

2.3 Second-Order Zeeman effect and Temperature-Independent Paramagnetism

In deriving the van Vleck equation, we used the energy levels of the isolated system (*i.e.* in the absence of a magnetic field) as a starting point, and assumed that all other states were so high up in energy that we could safely ignore them. However, we don't have an isolated system - we have a system in a magnetic field, and the additional Zeeman term in the Hamiltonian means that the wavefunctions will be slightly different from those in the truly isolated system. We deal with this quantum mechanically through perturbation theory - we solve the system for the simpler case (without the magnetic field) and then we use the wavefunctions for this isolated system to calculate the effect of the field. In the language of perturbation theory, we say that the magnetic field 'mixes in' higher lying states. The mixing in of excited states by the magnetic field is called '*Temperature-Independent Paramagnetism*' or *TIP* for short. It is always present, and it *always* has the effect of increasing the susceptibility. If there are other sources of paramagnetism (unpaired electrons), TIP is usually a small factor, but it can be large if there are low-lying excited states. A good example is CrO_4^{2-}, which has no unpaired electrons (d^0), and so should be diamagnetic. In fact, at room temperature it has $\mu_{eff} \sim 0.6\mu_B$ due to the mixing in of low-lying LMCT states by the magnetic field.

$$\chi_{TIP} = \frac{2\mu_0 N_A \alpha \mu_B^2}{\Delta}$$

where Δ is the excitation energy. α =4 for states of E symmetry, 2 for states of A_2 symmetry and 0 for states of A_1 symmetry. So for systems where the Curie law is a good first approximation, we can add a small TIP term to the susceptibility:

$$\boxed{\chi_{mol} = \frac{N_A \mu_0}{3kT}\mu_{SO}^2 + \frac{2N_A \mu_0 \alpha \mu_B^2}{\Delta}} \tag{2.3.1}$$

It is very important to appreciate that TIP is a temperature-independent contribution *to the susceptibility*, χ. This means that when we convert χ to μ by multiplying by T, the effect of TIP is temperature-dependent ($\mu_{eff} \propto \sqrt{\chi_{mol} T}$).

The effect of TIP on plots of χ, χ^{-1} and μ_{eff} for a Curie-law paramagnet is shown in Figure 2.6: the small additional TIP component makes a constant addition to χ that is really only perceptible at high temperatures, where the first term in Equation 2.3.1 is small. The deviation is more apparent in χ^{-1}, where the line curves below the straight-line plot characteristic of the Curie law. Finally, μ_{eff} increases with temperature.

TIP is usually a small factor, and the plots in Figure 2.6 are an exaggeration of the magnitude in typical systems. Nevertheless, TIP is always there in the background, and, as we see later, it becomes important if we want to understand some rather subtle trends.

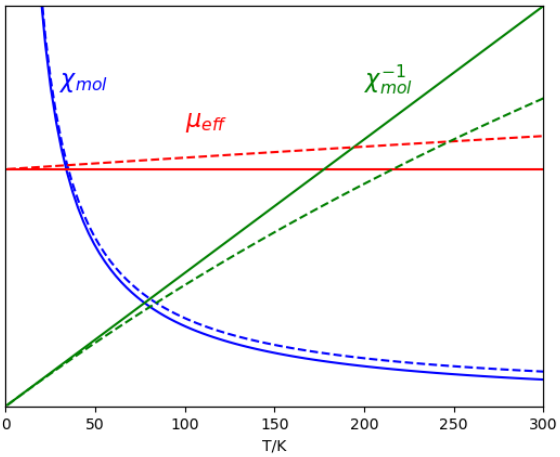

Figure 2.6: Temperature-Independent Paramagnetism. Full lines indicate the Curie-law plots in the absence of TIP.

2.4 Complexes with ground-state orbital angular momentum.

2.4.1 Orbital angular momentum and magnetism

The Zeeman operator acts on both the spin (Equation 2.2.2) and orbital (Equation 2.2.3) angular momenta. The orbital Zeeman effect can be understood in a qualitative way by noting that the angular momentum operators $\hat{l_x}, \hat{l_y}, \hat{l_z}$ induce rotations between orbitals (Figure 2.7).
In order to have non-zero orbital angular momentum, we need to meet all three of the following requirements:

1. Two (or more) orbitals are degenerate
2. The two orbitals must be unequally occupied.
3. The two orbitals must be related by a rotation about an axis.

In the ^2D state of a d^1 atom or ion, for example, d_{xy} and $d_{x^2-y^2}$ are degenerate, and only one of them can be occupied at a time as there is only one electron. The two orbitals are related by a rotation about z, so the two conditions are met.

Orbital angular momentum provides another source of magnetic susceptibility, but also leads to temperature-dependence through spin-orbit coupling. Spin-orbit coupling splits the $\{S, L\}$ manifold into levels defined by the total angular momentum, J, and the splitting is often of the order of kT. The population of states with different alignment of L and S relative to the field can therefore change with temperature.

There are two common classes of system that have ground-state orbital angular momentum: f-elements (lanthanides) and transition metal complexes with T-symmetry ground states (T_{1g}, T_{2g}, T_2 *etc.*)

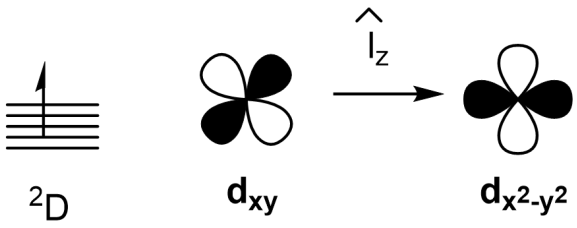

Figure 2.7: The origin of orbital angular momentum.

2.4.2 Magnetism of the lanthanides ions

Consider Pr^{3+}, with an f^3 configuration - following Hunds' rules, the ground-state term is ^3H, and the lowest-lying state is the one with lowest J, $J = 4$ (because the shell is less than half filled). In Pr^{3+}, the spin-orbit coupling constant $\lambda = 420$ cm^{-1}, and so the splitting between $J = 4$ and $J = 5$ is $5\lambda = 2100$ cm^{-1}, large enough to leave the ground state effectively isolated (Figure 2.8). Note the Landé interval rule, which states that the splitting $E(J+1) - E(J) = (J+1)\lambda$.

The problem is now very similar to the one in Figure 2.4, with an energetically isolated ground state, but now the effect of the magnetic field is more complex because we need to take into account both orbital and spin angular momentum, noting the anomalous g_e value of 2. By analogy with equations 2.2.3 and 2.2.2, The M_J sub-levels split in a magnetic field according to the Landé formula:

$$E(M_J) = \langle M_J|\hat{H}|M_J\rangle = g_J M_J \mu_B H$$

$$\mu_{eff} = g_J\sqrt{J\,(J+1)}$$

where

$$g_J = 1 + \frac{J\,(J+1) - L\,(L+1) + S\,(S+1)}{2J\,(J+1)} = \frac{3}{2} + \frac{S\,(S+1) - L\,(L+1)}{2J\,(J+1)} \qquad (2.4.1)$$

The room-temperature magnetic moments of the Ln^{3+} ions are summarised in Figure 2.9 and Table 2.3. The agreement between experiment and the predicted values based on the Landé formula is remarkably good in all cases other than Sm^{3+}, where the agreement is moderate, and Eu^{3+}, where it is spectacularly bad!

The agreement with the spin-only formula is very bad indeed for all but Gd^{3+} - the failure of the spin-only formula is not really a surprise because the core-like properties of the $4f$ orbitals mean that the ligands do not 'quench' the angular momentum. Gd^{3+} has an f^7 configuration (a half-filled shell) so there is no orbital angular momentum to quench, so the spin-only formula necessarily applies. More on quenching later.

Why, then, does the Landé formula appear to break down for Sm^{3+} and particularly for Eu^{3+}? The underlying reason can be traced to the Landé interval rule: $E(J+1) - E(J) = (J+1)\lambda$ is at its lowest when the ground-state J value is small, and in these circumstances the assumption that the

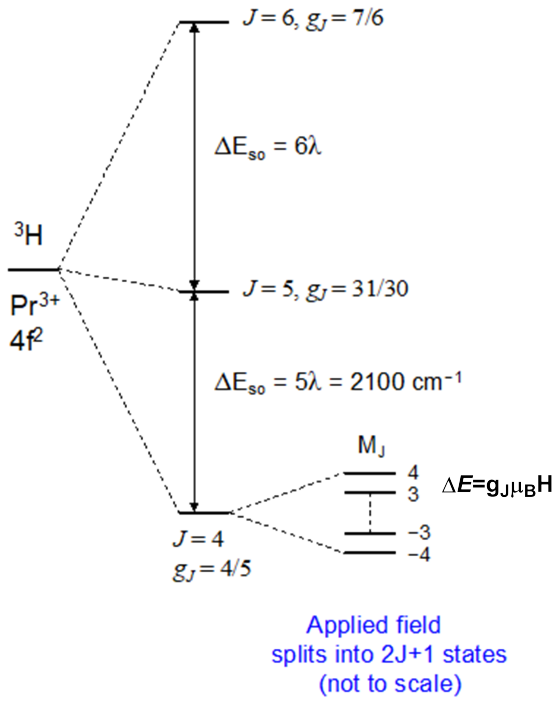

Figure 2.8: Splitting of the ground-state ^3H term of Pr^{3+} by spin-orbit coupling, and then of the ground $J = 4$ state by the magnetic field.

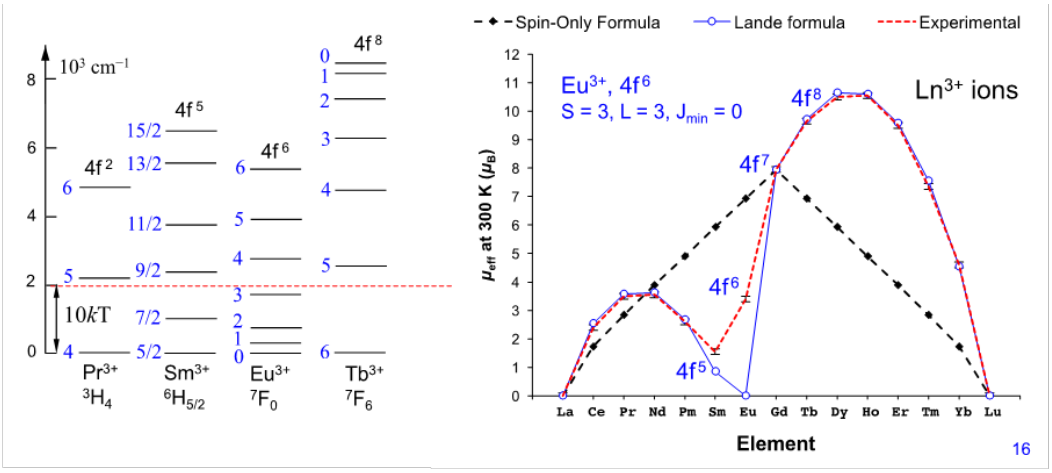

Figure 2.9: Magnetic moments of the lanthanide ions at room temperature

ground state is effectively isolated breaks down. So for the $^7F_0$ ground state of Eu^{3+}, the $J = 1$ excited state (which is not taken into account in any way in deriving the Landé formula) is only λ

Table 2.3: **Magnetic moments of the lanthanide ions.**

lanthanide ion	Configuration	Ground state	Unpaired e^-	$\mu_{eff} = g_J\sqrt{J\,(J+1)}$	Observed
La^{3+}	$4f^0$	$^1S_0$	0	0	0
Ce^{3+}	$4f^1$	$^2F_{5/2}$	1	2.54	2.3-2.6
Pr^{3+}	$4f^2$	$^3H_4$	2	3.58	3.4-3.6
Nd^{3+}	$4f^3$	$^4I_{9/2}$	3	3.62	3.5-3.6
Pm^{3+}	$4f^4$	$^5I_4$	4	2.68	-
Sm^{3+}	$4f^5$	$^6H_{5/2}$	5	0.85	1.4-1.7
Eu^{3+}	$4f^6$	$^7F_0$	6	0	3.3-3.5
Gd^{3+}	$4f^7$	$^8S_{7/2}$	7	7.94	7.9-8.0
Tb^{3+}	$4f^8$	$^7F_6$	6	9.72	9.5-9.8
Dy^{3+}	$4f^9$	$^6H_{15/2}$	5	10.65	10.4-10.6
Ho^{3+}	$4f^{10}$	$^5I_8$	4	10.60	10.4-10.7
Er^{3+}	$4f^{11}$	$^4I_{5/2}$	3	9.58	9.4-9.6
Tm^{3+}	$4f^{12}$	$^3H_6$	2	7.56	7.1-7.6
Yb^{3+}	$4f^{13}$	$^2F_{7/2}$	1	4.54	4.3-4.9
Lu^{3+}	$4f^{14}$	$^1S_0$	0	0	0

higher in energy. This has two consequences:

1. The $J = 1$ state can become thermally populated at elevated temperatures.
2. TIP (mixing of $J = 0$ and $J = 1$ by the magnetic field) becomes significant because of its dependence on $\frac{1}{\Delta E}$.

2.4.3 Transition metal complexes with T ground states.

In the majority of transition metal complexes, the ligand field is said to 'quench' the orbital angular momentum. So, for example, a free Cr^{3+} ion has a ^4F ground state so most certainly has orbital angular momentum, but when we put the ion in an octahedral ligand field, we find almost no trace of the orbital angular momentum in the measured magnetic moment - it corresponds very well to the spin-only value. So what has happened to the orbital contribution, which proved to be so important in the lanthanides?

A physical picture may help: imagine the orbital angular momentum of the d-electrons to be analogous to a spinning bike wheel. The ligands are like sticks, poked into the spokes, stopping it spinning. This happens in transition metals but not lanthanides because the nd orbitals protrude beyond the core and so interact with the ligands while the nf orbitals do not.

For a more rigorous quantum mechanical perspective, recall the necessary ingredients for the existence of orbital angular momentum set out in Figure 2.7. We require that:

1. two or more d orbitals are degenerate
2. the occupancy of these two orbitals must be different
3. it must be possible to convert one orbital, ψ_1, into another, ψ_2, by a rotation about one or more axes. This ensures that the matrix element $\langle\psi_1|\,\hat{l}_i\,|\psi_2\rangle$ is not zero

The ligands partially lift the degeneracy of the orbitals (from 5-fold to 3 and 2 in cubic point groups) and so this immediately reduces the possibility of meeting the three criteria. In fact, the only major class of complexes where orbital angular momentum is retained is when the ground state has T-symmetry. Even after the ligand field has split the d levels into t_{2g} and e_g sets, it remains possible to convert *e.g.* d_{xz} to its degenerate partner d_{yz} *via* a rotation about z. So as long as one is occupied and the other is not (and this is the necessary condition for the state to have T symmetry!), we have all the ingredients for orbital angular momentum.

So why does this not work for E states? These have an unequal population of two degenerate orbitals, so certainly meet criteria 1 and 2, above. However, an inspection of the orbitals (d_{z^2} and $d_{x^2-y^2}$) immediately shows that there is no rotation that can convert one into the other - they are just completely different shapes. Quantum mechanically, this difference in shape emerges from the composition of the orbitals: $d_{z^2} = |0\rangle$ while $d_{x^2-y^2} = \frac{1}{\sqrt{2}}\left(|2\rangle + |-2\rangle\right)$ and the difference of 2 in the m_l values prevents them from being mixed by $\hat{l}_i$.[6]

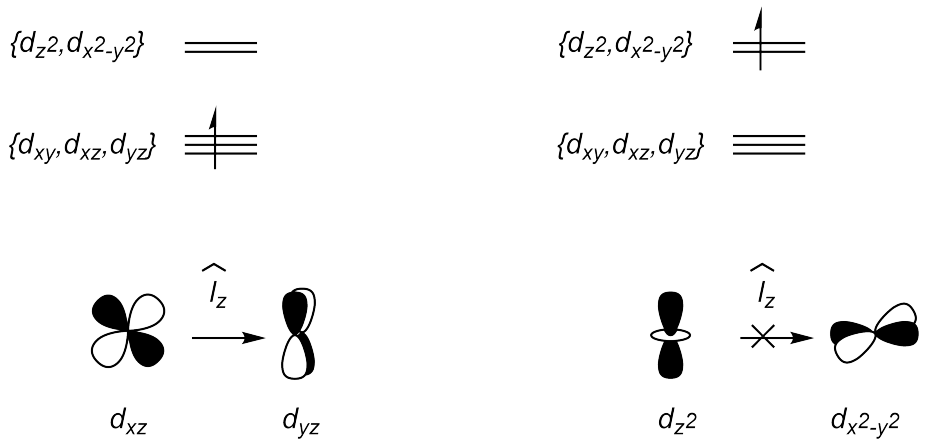

Figure 2.10: Orbital angular momentum for T and E states

The '$t_2 - p$ isomorphism' and splitting of the J states The three t_{2g} orbitals look and behave very much like a set of three p orbitals, in so much as they have a residual orbital angular momentum

[6]It is often stated that "states with E symmetry do not have ground state orbital angular momentum" (for the reasons given above). However, this should be qualified to read "*cubic* (*i.e.* octahedral or tetrahedral) E states do not have orbital angular momentum". Consider, for example, a *trans*-ML_4X_2 complex with D_{4h} symmetry. In this case the $d_{xy,xz}$ pair transform as e_g, and so a ^2E_g state arising from a $d^1_{xz}d^0_{yz}$ or $d^2_{xz}d^1_{yz}$ configuration does have orbital angular momentum.

$L = 1$. Combined with the $S = 1/2$ of the ${}^2T_{2g}$ ground of a ${t_{2g}}^1$ ion (Ti^{3+}, for example), this gives states with $J = 1/2$ and $J = 3/2$. According to Hund's rule, we should expect $J = 1/2$ to be lowest for a less-than-half-filled shell (and indeed that is what we would see for a p^1 system), but in fact we see the opposite: $J = 3/2$ is the ground state, $\frac{3}{2}\zeta$ below the $J = 1/2$ excited state. The analogy between t_2 and p is not exact - the action of the angular momentum operators is subtly different and this causes the reversal in the energy of the states.

With the spin-orbit coupling accounted for, the situation in the second column of Figure 2.11 appears very much like the Pr^{3+} case, and we can apply the van-Vleck formula in the usual way. There is, however, a further consequence of the *isomorphism*, rather than exact analogy, between p and t_{2g} - the formula for the Landé g_J factor is different:

$$g_J = \left| -1 + 3\left[\frac{J(J+1) - L(L+1) + S(S+1)}{2J(J+1)}\right]\right| \tag{2.4.2}$$

There is no need to remember this, but plug in relevant values ($J = 3/2$, $L = 1$, $S = 1/2$) and you should get $g_J = 0$ for the $J = 3/2$ ground state. The $J = 1/2$ state, in contrast, has $g_J = 2$, so it is split in a magnetic field. The fact that $g_J = 0$ means that the ground state is not affected by the magnetic field to first order: it is 'non-magnetic', and at very low temperatures, the magnetic moment, μ_{eff}, approaches zero.

Despite the apparent similarities between Pr^{3+} (Figure 2.8) and octahedral Ti^{3+} (Figure 2.11), the magnitude of the spin-orbit coupling is very different: λ =520 cm^{-1} for the former but only 155 cm^{-1} for the latter. This means that the splitting between $J = 3/2$ and $J = 1/2$ in Ti^{3+} is only 230 cm^{-1} compared to 2100 cm^{-1} for the $J = 4$ and $J = 5$ states of Pr^{3+}. If the splitting of the ground- and excited spin-orbit states in Ti^{3+} was similar to that in Pr^{3+}, it would have a temperature-independent μ_{eff} of 0. In fact, the situation in Ti^{3+} is more comparable to Sm^{3+} or Eu^{3+} in Figure 2.9 than it is to Pr^{3+}, and we need to take into account thermal population of both $J = 3/2$ and $J = 1/2$ states to understand the magnetism over a wide temperature range.

The dependence of μ_{eff} on both temperature and on spin-orbit coupling constant is captured in the 'Kotani diagram' in Figure 2.12, where the independent variable is $\frac{kT}{\lambda}$. This choice of variable means that most first-row transition metals lie to the right of the plot (small λ) while most $4d$ and $5d$ elements lie to the left (large λ).

Although the behaviour is complex, we can understand at least the limiting behaviour at high and low temperatures.

At very low temperatures, only the $J = 3/2$ spin-orbit state is populated and, as we have seen, $g_J = 0$ and μ_{eff} is therefore also 0.

As T increases (or, equivalently, as λ gets smaller), two effects are in play:

1. the population of the excited $J = 1/2$ state increases. This state has $g_J = 2$, so is inherently 'more magnetic' than the ground state, and so μ_{eff} increases.

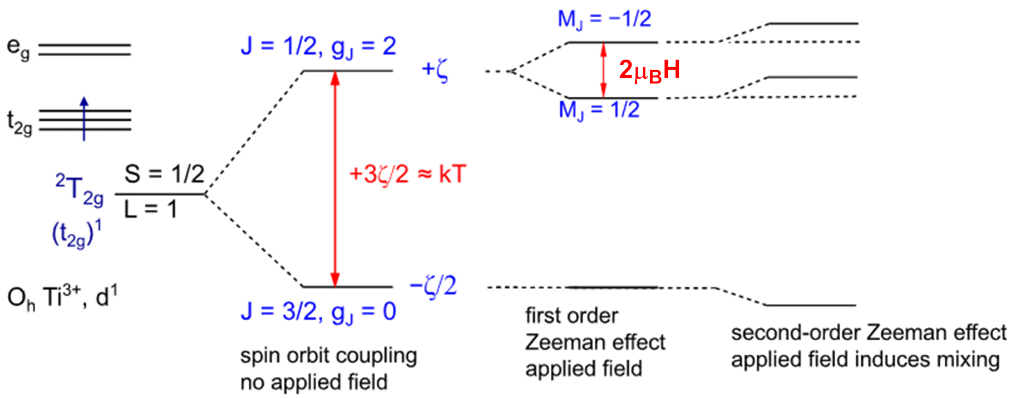

Figure 2.11: Splitting of the ${}^2T_{2g}$ ground state of a ${t_{2g}}^1$ ion. Note that the one-electron spin orbit coupling constant, ζ, is related to the many-electron analogue through $\lambda = \frac{\pm\zeta}{2S}$, where the + is for less than half-filled shells and the - for more than half-filled shells. In cases with one unpaired electron ($S = 1/2$), $\lambda = \pm\zeta$.

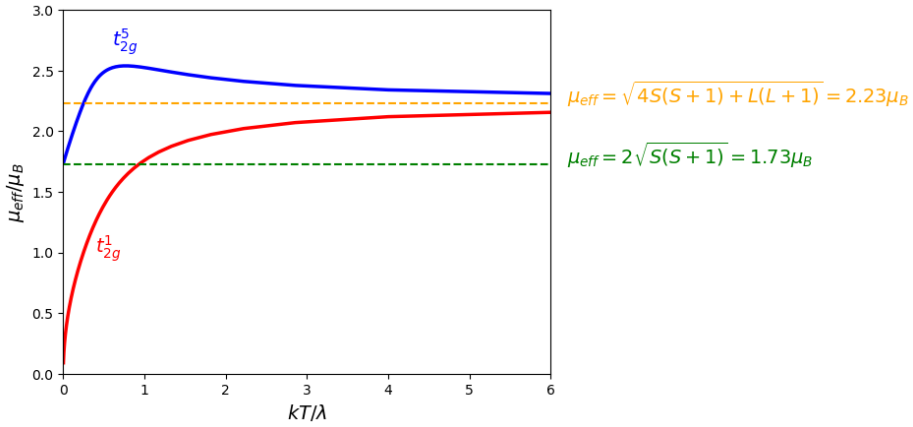

Figure 2.12: Kotani plots for octahedral d^1 and low-spin d^5 ions.

2. TIP ('second-order Zeeman effect' in Figure 2.11) becomes more pronounced (this is perhaps most obvious if we think of a shift to the right as representing a reduction in ζ, and therefore the separation of $J = 3/2$ and $J = 1/2$, rather than an increase in temperature).

The value of μ_{eff} rises to a limiting high-temperature (low-ζ) value of:

$$\mu_{eff} = 2.23\mu_B = \sqrt{4S\,(S+1) + L\,(L+1)}$$

Here, the orbital and spin angular momenta are effectively decoupled from each other, and make separate additive contributions to χ_{mol}.

It is often said that any agreement with the spin-only formula is coincidental when there is first-order orbital angular momentum. This is somewhat true - the green line in Figure 2.12 shows the spin-only value, which the curve passes through when $\frac{kT}{\lambda} \sim 1$: clearly, substantial deviations occur to either side of this.

However, the vast majority of first row transition metal complexes (small λ) lie to the right of the plot, where the curve is relatively flat. The limiting high-T (or low-ζ) value is $\mu_{eff} = 2.23\mu_B = \sqrt{4S(S+1) + L(L+1)}$. The origins of this formula are that the spin and orbital angular momenta are effectively decoupled from each other (this is easiest to see for $\zeta = 0$), and so they make separate, additive, contributions to χ.

L is always 1 (we are always concerned with T states), so $L(L+1) = 2$, and this term is often dominated by the spin contribution, $4S(S+1)$. Even for the ions here with only a single unpaired electron, $4S(S+1) = 3$ is already larger than $L(L+1)$, and for the ${}^5T_{2g}$ ground state of Fe^{2+}, $4S(S+1) = 24$! So first-row transition metals tend to have magnetic moments only a little above the spin-only formula even when they have T ground states, and the deviation becomes smaller the more unpaired electrons the ion has. So for the ${}^5T_{2g}$ state of high-spin Fe^{2+}, the spin-only value is 4.90 and $\sqrt{4S(S+1) + L(L+1)} = 5.10$. So the spin-only value is a fairly good approximation.

For ${}^2T_{2g}$ states arising from a ${t_{2g}}^5$ configuration, the ordering of the spin-orbit coupled levels is reversed, with the magnetic $J = 1/2$ state lying lowest ($g_J = 2$). Note that because $g_J = 2 = g_e$, the magnetic moment on the left hand side of the blue curve in Figure 2.12 (large ζ or very low temperature) is coincidentally equal to the spin only value of $1.73\mu_B$. As ζ decreases (or the temperature increases) we again approach the limiting value of $\mu_{eff} = \sqrt{4S(S+1) + L(L+1)} = 2.23\mu_B$. One interesting point to note is that the value of μ_{eff} actually goes above the value of 2.23 μ_B before dropping back down - this is again due to TIP.

Table 2.4: **Magnetic moments of the some transition metal ions with T ground states.**

Compound	ion	d^n	Geometry	Ground term	μ_{SO}/μ_B	$300K$	$80K$
$CsTi(SO_4)_2 \cdot 12\,H_2O$	Ti^{3+}	d^1	O_h	$^2T_{2g}$	1.73	1.84	1.55
ReF_6	Re^{6+}	d^1	O_h	$^2T_{2g}$	1.73	0.62	-
$(NH_4)V(SO_4)_2 \cdot 12\,H_2O$	V^{3+}	d^2	O_h	$^3T_{1g}$	2.83	2.80	2.78
$K_3Mn(CN)_6$	Mn^{3+}	d^4	O_h	$^3T_{1g}$	2.83	3.50	3.31
K_2RuCl_6	Ru^{4+}	d^4	O_h	$^3T_{1g}$	2.83	2.57	1.63
K_2OsCl_6	Os^{4+}	d^4	O_h	$^3T_{1g}$	2.83	1.50	0.78
$K_4Mn(CN)_6$	Mn^{2+}	d^5	O_h	$^2T_{2g}$	1.73	2.18	2.03
$K_3Fe(CN)_6$	Fe^{3+}	d^5	O_h	$^2T_{2g}$	1.73	2.25	1.90
$Ru(NH_3)_6Cl_3$	Ru^{3+}	d^5	O_h	$^2T_{2g}$	1.73	2.13	1.85
$Os(NH_3)_6Cl_3$	Os^{3+}	d^5	O_h	$^2T_{2g}$	1.73	1.81	-
$(NH_4)_2Fe(SO_4)_2 \cdot 6\,H_2O$	Fe^{2+}	d^6	O_h	$^5T_{2g}$	4.90	5.47	5.37
$(NH_4)_2Co(SO_4)_2 \cdot 6\,H_2O$	Co^{2+}	d^7	O_h	$^4T_{1g}$	3.87	5.10	4.60
$(NEt_4)_2NiCl_4$	Ni^{2+}	d^8	T_d	$^3T_1$	2.83	3.89	3.25

2.5 Complexes with $A_{2(g)}$ and $E_{(g)}$ ground states

2.5.1 Second-order Spin-Orbit Coupling (SOC).

The final set of complexes that we need to consider are those with A_2 and E ground states, shown in Figure 2.13. In the discussion of the residual orbital angular momentum of T states, we argued that the orbital angular momentum in E states is *quenched* because it is not possible to convert one of the e orbitals into the other by a rotation about any axis (the third of the three requirements). It is even more obvious that A_2 states do not have ground-state orbital angular momentum because the don't even pass the second test of having unequal occupation of the degenerate orbitals.

However, let's do a thought experiment where we make Δ very small compared to kT. We would now effectively restore the full degeneracy of all five d orbitals, and all three criteria required for orbital angular momentum would be met for both E and A_2 states. So orbital angular momentum is only quenched in the limit that $\Delta >> kT$. In the following examples, we look at what happens when Δ is small enough that some residual traces of orbital angular momentum persist.

Ground states with A_2 or E symmetry only arise for d^{1-4} and d^{6-9} configurations, and in all these cases there are excited states with T symmetry $\sim \Delta$ higher in energy (such as $^4T_{2g}$ and $^4T_{1g}$ that arise from the octahedral ${t_{2g}}^2{e_g}^1$ configuration, for example). These excited T states are certainly too high in energy to be thermally populated at any reasonable temperature, but, if Δ is not too large, they can be mixed into the ground A_2 or E state by *second-order spin-orbit coupling* - in effect the ground state acquires a small amount of T character, and that increases or decreases χ depending on whether the shell is more than or less than half filled. 'Second-order' here reflects the fact that the orbital angular momentum is not present in the ground state, as it was in the systems with T ground states.[7]

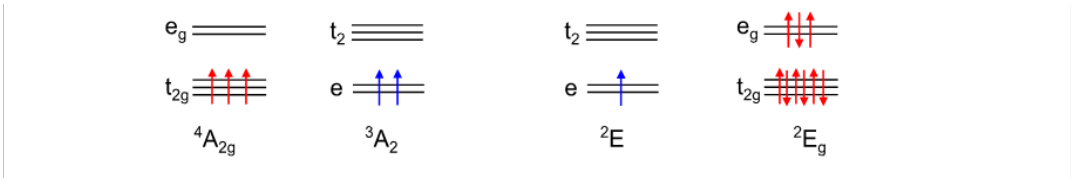

Figure 2.13: Configurations that generate A_2 and E ground states.

The effect of a magnetic field on the $^4A_{2g}$ state is shown in Figure 2.14. If we ignore spin-orbit coupling (left hand side) then the situation is precisely as it was for the Curie-law paramagnet in Figure 2.4: the M_S levels are split by $g_e\mu_B H$ where $g_e \sim 2.0$. If we then introduce spin-orbit coupling (right-hand side), the effect is to mix a small amount of the $^4T_{2g}$ state into the ground state. When we subsequently apply the magnetic field, the Zeeman splitting of the M_S levels of the ground state is slightly different from what it would be without the mixing, reflecting the fact that it now has a small amount of orbital angular momentum through the admixture of the $^4T_{2g}$ state.

[7]The phrase 'mixing in' is perturbation theory jargon - the spin-orbit coupling was always present, but we chose to ignore it in the first approximation, when we applied the ligand field to split the d levels into t_{2g} and e_g and then introduced $e-e$ repulsions to form singlets and triplets. By adding spin-orbit coupling in retrospectively using perturbation theory ('to second order'), we are simply correcting its earlier omission.

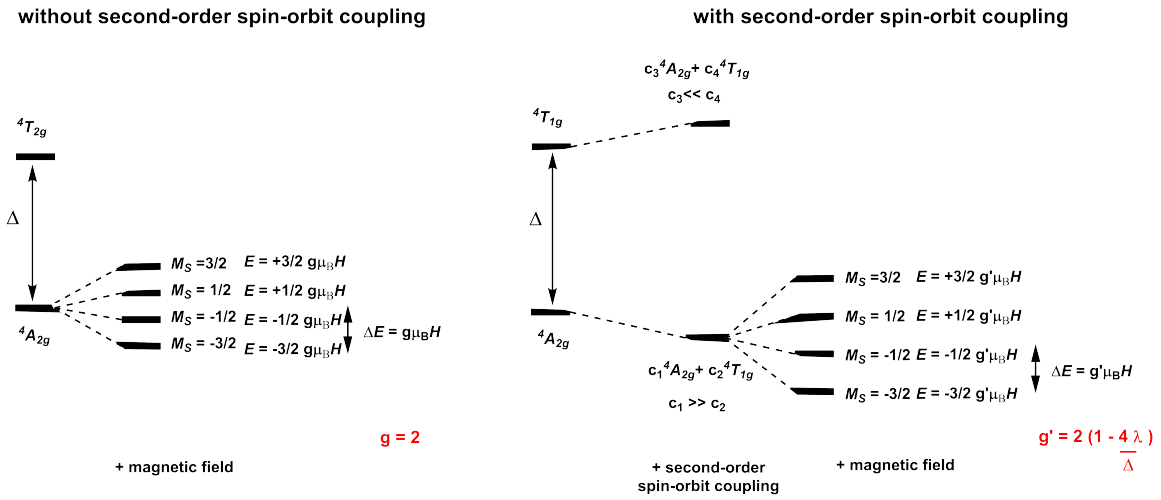

Figure 2.14: The influence of second-order spin-orbit coupling on the magnetic properties of the $^4A_{2g}$ ground state of the d^3 configuration.

The expression for the g factor is:

$$g' = 2\left(1 - \frac{\alpha\lambda}{\Delta}\right)$$

where λ is the spin-orbit coupling constant and Δ is the ligand-field splitting. α is 4 for $A_{2(g)}$ states and 2 for $E_{(g)}$ states. Clearly the effects of spin-orbit coupling will be significant when either Δ is small (low-lying excited states) or when λ is large (heavy transition metals). Conversely, when $\lambda = 0$ or Δ is very large, $g' = 2$.

The modification of the g factor feeds into a modification of the expression for the susceptibility, χ:

$$\chi_{mol} = \frac{N_A \mu_0 \mu_{SO}^2}{3kT}\left(1 - \frac{\alpha\lambda}{\Delta}\right)^2$$

and a modified expression for the effective magnetic moment:

$$\boxed{\mu_{eff} = \mu_{SO}\left(1 - \frac{\alpha\lambda}{\Delta}\right)} \qquad (2.5.1)$$

λ is positive for less than half-filled shells, and so these second-order effects lead to a *reduction* in μ_{eff} while for more than half-filled shells λ is negative and they lead to an *increase* in μ_{eff}. The influence of second-order spin-orbit coupling on χ, χ^{-1} and μ_{eff} is shown in the middle column of Figure 2.15, for less-than and more-than half-filled shells. The corresponding plot for the Curie-law and Curie-law+TIP are also shown again for comparison. The modification of the g factor changes

the constant in the Curie law plot ($\chi = \frac{C'}{T}$), and so changes the gradient of the χ^{-1} plot. μ_{eff} remains independent of temperature, but its value is raised compared to the spin-only value for more than half-filled shells and lowered for less than half-filled shells.

2.5.2 Second-order SOC and TIP

The effects of second-order spin-orbit coupling are, in many ways, similar to the Temperature-Independent Paramagnetism discussed previously. Both depend on the mixing in of excited states, so both will be significant when these excited states are low-lying. The difference between the two lies in the mechanism of the mixing: for second-order spin-orbit, the excited states are mixed in by the spin-orbit coupling operator, and this is an intrinsic property of the molecule (spin-orbit coupling is always present - we just chose to ignore it in the first approximation!). With TIP, it is the magnetic field that induces the mixing, and so this is obviously only a factor when the molecule is actually in a field. The two effects are additive, but the effects of second-order spin-orbit coupling on χ are temperature dependent while those of TIP are temperature independent:

$$\chi_{mol} = \frac{N_A \mu_0 \mu_{SO}^2}{3kT}\left(1 - \frac{\alpha\lambda}{\Delta}\right)^2 + \frac{2\mu_0 N_A \alpha \mu_B^2}{\Delta} \tag{2.5.2}$$

The combined effects of second-order SOC and TIP are shown in the final plots on the right-hand side of Figure 2.15. In the case of more than half-filled shells, both effects increase μ_{eff}, and the result is a significant upward deviation from the spin-only value. For less than half-filled shells, the two effects counteract each other - TIP increases μ_{eff} while second-order spin-orbit decreases it. In some cases they cancel out almost perfectly, giving μ_{eff} values very close to the spin-only ones.

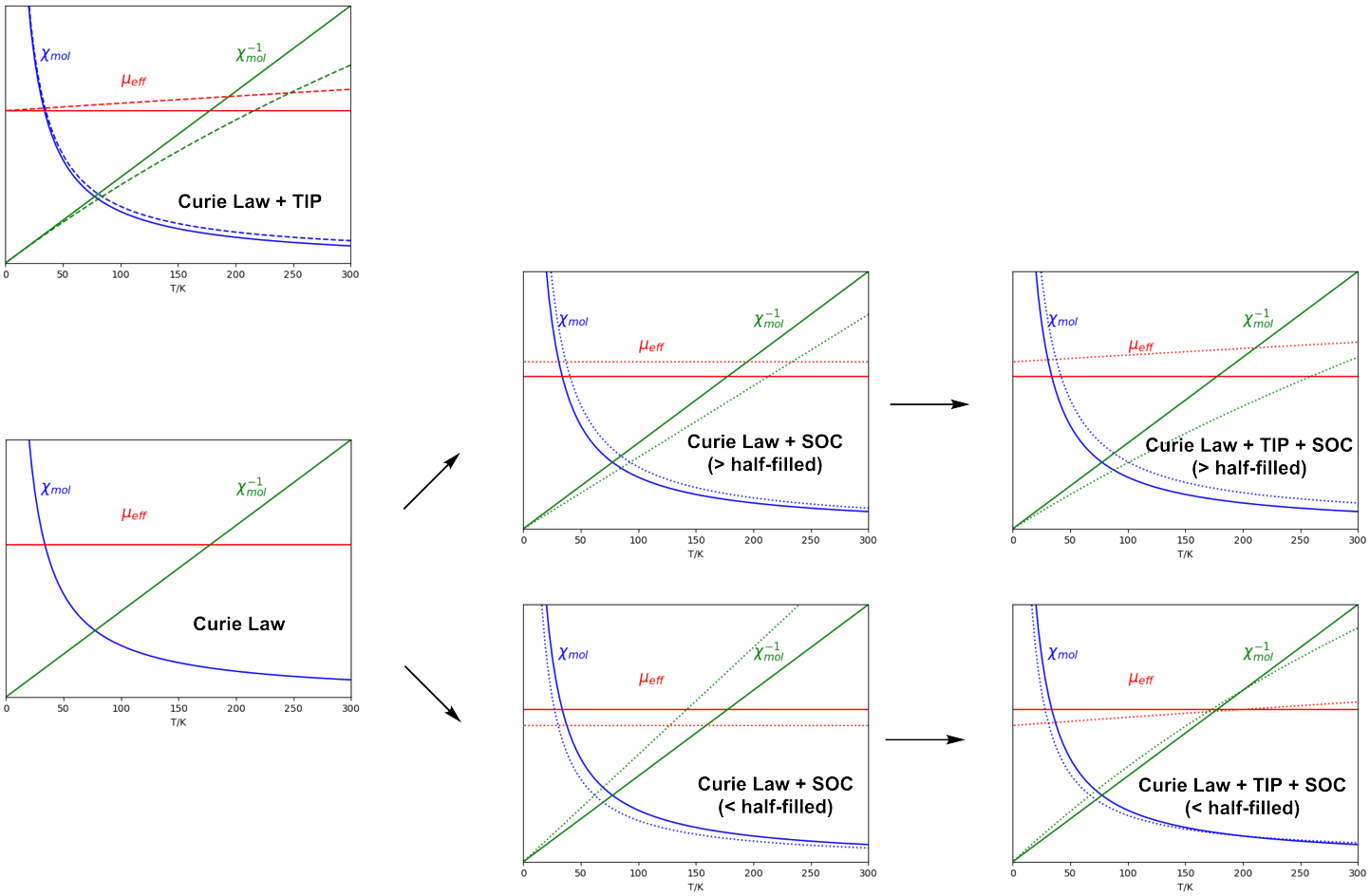

Figure 2.15: Summary of the effects of second-order spin-orbit coupling and TIP on χ, χ^{-1} and μ_{eff}

The magnetic properties of a wide range of complexes with A_2 and E ground states are summarised in Table 2.5. Points to pick out from this data:

1. All values are independent or only very weakly dependent on temperature. Any weak temperature dependence (in μ_{eff}) comes from the TIP term.
2. Deviations from the spin-only values are small for less than half-filled shells, where TIP and second-order SOC cancel each other out (at least approximately), but rather more for more than half-filled shells where the two reinforce each other.
3. The exact agreement between measured μ_{eff} and μ_{SO} for K_2FeO_4 arises from a coincidental exact cancellation of second-order SOC and TIP terms.
4. In $[Re(NCS)_6]^{2-}$, second-order SOC is relatively large because λ is large. The reduction in μ_{eff} due to second-order SOC therefore dominates the increase due to TIP (which does not depend on λ) and we see a significant reduction in μ_{eff} below μ_{SO}.
5. In the d^7 series, the deviation from μ_{SO} increases as the ligand-field splitting, Δ_t, decreases: excited states are lower-lying, so both second-order SOC and TIP become larger.

Table 2.5: **Magnetic properties of the some transition metal ions with A_2 and E ground states.**

Complex	d^n	μ_{SO}	μ_{eff}/μ_B
VCl_4	1	1.73	1.69
K_2FeO_4	2	2.83	2.83
$Cr(SO_4)\cdot 6\,H_2O$	4	4.90	4.84
$(NEt_4)_2[FeCl_4]$	6	4.90	5.40
$(NH_4)_2Ni(SO_4)_2\cdot 6\,H_2O$	8	2.83	3.23
$K_2Cu(SO_4)_2\cdot 6\,H_2O$	9	1.73	1.91

Octahedral d^3 - less than half-filled shell, $^4A_{2g}$

Complex	μ_{SO}	μ_{eff}/μ_B
$CrCl_3$	3.87	3.90
$[Cr(NH_3)_6]^{3+}$	3.87	3.77
$[Cr(bipy)_3]^{3+}$	3.87	3.81
$[Cr(CN)_6]^{3-}$	3.87	3.87
$[MnCl_6]^{2-}$	3.87	3.84
$[Mo(bipy)_3]^{3+}$	3.87	3.66
$[Re(NCS)_6]^{2-}$	3.87	3.40

Tetrahedral d^7 - more than half-filled shell, $^4A_2$

Complex	μ_{SO}	μ_{eff}/μ_B	Δ_t (cm^{-1})
$[Co(NCS)_4]^{2-}$	3.87	4.36-4.53	4550
$[Co(NCO)_4]^{2-}$	3.87	4.38	4150
$[Co(N_3)_4]^{2-}$	3.87	4.47	3920
$[Co(SPh)_4]^{2-}$	3.87	4.50	3870
$[CoCl_4]^{2-}$	3.87	4.66-4.80	3130
$[CoBr_4]^{2-}$	3.87	4.80-4.87	2850
$[CoI_4]^{2-}$	3.87	4.87-5.01	2650

3 Appendix: Character tables, direct product tables and descent in symmetry tables

3.1 Character tables for O_h, T_d, C_{4v}

Table 3.6: Character Table for O_h

O_h	E	$8C_3$	$6C_2$	$6C_4$	$3C_2$	i	$6S_4$	$8S_6$	$3\sigma_h$	$6\sigma_d$		
A_{1g}	1	1	1	1	1	1	1	1	1	1		$x^2+y^2+z^2$
A_{2g}	1	1	-1	-1	1	1	-1	1	1	-1		
E_g	2	-1	0	0	2	2	0	-1	2	0		$(2z^2-x^2-y^2,\, x^2-y^2)$
T_{1g}	3	0	-1	1	-1	3	1	0	-1	-1	(R_x, R_y, R_z)	
T_{2g}	3	0	1	-1	-1	3	-1	0	-1	1		$(xy,\, xz,\, yz)$
A_{1u}	1	1	1	1	1	-1	-1	-1	-1	-1		
A_{2u}	1	1	-1	-1	1	-1	1	-1	-1	1		
E_u	2	-1	0	0	2	-2	0	1	-2	0		
T_{1u}	3	0	–1	1	–1	-3	-1	0	1	1	(x, y, z)	
T_{2u}	3	0	1	-1	–1	-3	1	0	1	-1		

Table 3.7: Character Table for T_d

T_d	E	$8C_3$	$3C_2$	$6S_4$	$6\sigma_d$		
A_1	1	1	1	1	1		$x^2+y^2+z^2$
A_2	1	1	1	–1	–1		
E	2	–1	2	0	0		$(2z^2-x^2-y^2,\, x^2-y^2)$
T_1	3	0	–1	1	–1	(R_x, R_y, R_z)	
T_2	3	0	–1	–1	1	(x, y, z)	$(xy,\, xz,\, yz)$

Table 3.8: Character Table for C_{4v}

C_{4v}	E	$2C_4$	C_2	$2\sigma_v$	$2\sigma_d$		
A_1	1	1	1	1	1	z	z^2,x^2+y^2
A_2	1	1	1	-1	–1		
B_1	1	–1	1	1	-1		x^2-y^2
B_2	1	–1	1	–1	1		xy
E	2	0	–2	0	0	(x,y)	(xz,yz)

3.2 Descent in symmetry tables

Table 3.9: Descent in symmetry table from R_3 to O, D_6, D_5, D_4 and D_3

R_3	O	D_6	D_5	D_4	D_3
S	A_1	A_1	A_1	A_1	A_1
P	T_1	A_2+E_1	A_2+E_1	A_2+E	A_2+E
D	$E+T_2$	$A_1+E_1+E_2$	$A_1+E_1+E_2$	$A_1+B_1+B_2+E$	A_1+2E
F	$A_2+T_1+T_2$	$A_2+B_1+B_2+2E$	A_1+2A_2+2E		
G	$A_1+E+T_1+T_2$	$2A_1+A_2+B_1+B_2+2E$	$2A_1+A_2+3E$		
H	$E+2T_1+T_2$	$A_1+2A_2+B_1+B_2+3E$	A_1+2A_2+4E		

3.3 Direct product tables

Table 3.10: Direct products for the T_d, T, O_h and O point groups.

	A_1	A_2	E	T_1	T_2
A_1	A_1	A_2	E	T_1	T_2
A_2		A_1	E	T_2	T_1
E			$A_1+[A_2]+E$	T_1+T_2	T_1+T_2
T_1				$A_1+E+[T_1]+T_2$	$A_2+E+T_1+T_2$
T_2					$A_1+E+[T_1]+T_2$